UNIVERSITY OF KWAZULU-NATAL

Performance Analysis and Enhancement Schemes for Spatial Modulation

Nigel Reece Naidoo

2010

Performance Analysis and Enhancement Schemes for Spatial Modulation

By Nigel Reece Naidoo

Submitted in fulfilment of the academic requirements
for the degree of M.S.c Engineering
in the Faculty of Engineering
at the University of KwaZulu-Natal, Durban, South Africa

December 2010

As the candidate's supervisor I have approved this dissertation for submission.

Signed: _____

Name: Professor HongJun Xu

Date: 17 December 2010

Declaration

I, Nigel Reece Naidoo, declare that

i. The research reported in this thesis, except where otherwise indicated, is my original work.
ii. This thesis has not been submitted for any degree or examination at any other university.
iii. This thesis does not contain other persons' data, pictures, graphs or other information, unless specifically acknowledged as being sourced from other persons.
iv. This thesis does not contain other persons' writing, unless specifically acknowledged as being sourced from other researchers. Where other written sources have been quoted, then:
    a. their words have been re-written but the general information attributed to them has been referenced;
    b. where their exact words have been used, their writing has been placed inside quotation marks, and referenced.
v. Where I have reproduced a publication of which I am an author, co-author or editor, I have indicated in detail which part of the publication was actually written by myself alone and have fully referenced such publications.
vi. This thesis does not contain text, graphics or tables copied and pasted from the Internet, unless specifically acknowledged, and the source being detailed in the thesis and in the References sections.

Signed: _____

Acknowledgements

Firstly, I would like to sincerely thank my supervisor, Prof HongJun Xu, who has spent countless hours guiding me through this degree. His extraordinary work ethic and passion for research is unparalleled. Secondly, I extend my full appreciation to Dr Tahmid Quazi, for his significant contribution in reviewing this dissertation.

I would like to thank my family and friends for their continued support and encouragement over the past two years. I would like to thank my mother in particular for helping me through the most stressful of times.

To my girlfriend, Alicia, thank you for all the love and inspiration that you have given me.

I also acknowledge the National Research fund (NRF) for their initial financial assistance in this project. The opinions expressed and conclusions arrived at, are not necessarily attributed to the NRF.

Lastly, many thanks go to Telkom SA for their support in this project.

Abstract

Multiple-input multiple-output (MIMO) technology has emerged as a popular technique for enhancing the reliability and capacity of wireless communication systems. In this dissertation, we analyze the spatial modulation (SM) MIMO technique and investigate possible extensions to this scheme.

To date, there has been no literature reporting on the theoretical performance of M-ary quadrature amplitude modulation (M-QAM) SM with maximum likelihood (ML) based detection. The first objective of this dissertation is to present an asymptotic bound to quantify the average bit error rate (BER) of M-QAM SM with ML detection over independent and identically distributed (i.i.d) Rayleigh flat fading channels. The analytical frameworks are validated by Monte Carlo simulation results, which show the derived bounds to be tight for high signal-to-noise ratio (SNR) values.

The ML based SM detector is optimal, since it offers the best detection performance. However, this technique is not practical due to its high computational complexity. The second objective of this dissertation is to introduce a novel SM detection scheme, termed multiple-stage (MS) detection. Performance and complexity comparisons with existing SM detectors show two main benefits of MS detection: near optimal BER performance and up to a 35% reduction in receiver complexity as compared to the ML based detector.

Conventional SM schemes are unable to exploit the transmit diversity gains provided by the MIMO channel. The third objective of this dissertation is to propose Alamouti coded spatial modulation (ACSM), a novel SM based scheme with transmit diversity. The ACSM technique combines SM with Alamouti space-time block coding (STBC), thereby improving the diversity aspect and overall system performance of conventional SM. A closed form expression for the average BER of real constellation ACSM over i.i.d Rayleigh flat fading channels is derived and Monte Carlo simulations are used to verify the accuracy of this analytical expression. The BER performance of ACSM is compared to that of SM and Alamouti STBC. Simulation results show that the new scheme outperforms SM and Alamouti STBC by approximately 5.5 dB and 1.5 dB respectively, albeit at the cost of increased receiver complexity.

Table of Contents

List of Figures

List of Tables

List of Symbols

x	scalar quantity x
$\|x\|$	absolute value of x
x^*	complex conjugate of x
$\boldsymbol{x}$	vector $\boldsymbol{x}$
$\boldsymbol{x}^T$	transpose of $\boldsymbol{x}$
$\|\boldsymbol{x}\|_F$	Frobenius norm of $\boldsymbol{x}$
$\boldsymbol{x}^H$	Hermitian (conjugate transpose) of $\boldsymbol{x}$
$\boldsymbol{X}$	matrix $\boldsymbol{X}$
$*$	the convolution operator
$\approx$	approximately equal to
$E_x[A]$	statistical expectation of A with respect to x
$Re\{\cdot\}$	the real part of a complex variable
$\underset{x}{argmin} \quad f(x)$	the value of x that minimizes the function $f(x)$
$\underset{x}{argmax} \quad f(x)$	the value of x that maximizes the function $f(x)$
$\mathcal{N}(\mu, \sigma^2)$	Gaussian distribution with mean μ and variance σ^2
$\mathcal{CN}(\mu, \sigma^2)$	complex Gaussian distribution with mean μ and variance σ^2. Note the real and imaginary components of the random variable are independent and are distributed according to $\mathcal{N}\left(\mu, \frac{\sigma^2}{2}\right)$

List of Acronyms

ACSM	Alamouti coded spatial modulation
AI	antenna index
AWGN	additive white Gaussian noise
BER	bit error rate
bps	bits per second
BPSK	binary phase shift keying
CSI	channel state information
dB	decibels
FBE-SM	fractional bit encoded spatial modulation
GRV	Gaussian random variable
GSSK	generalized space shift keying
HD	high definition
IAS	inter-antenna synchronization
ICI	inter-channel interference
i.i.d	independent and identically distributed
LOS	line of sight
MIMO	multiple-input multiple-output
ML	maximum likelihood
M-QAM	M-ary quadrature amplitude modulation
MRRC	maximal-ratio receiver combining
MS	multiple-stage

NMRC	normalized maximum ratio combining
OFDM	orthogonal frequency division multiplexing
OSM	optical spatial modulation
PDF	probability density function
PEP	pairwise error probability
SER	symbol error rate
SIMO	single-input multiple-output
SM	spatial modulation
SM-OD	spatial modulation with optimal detection
SNR	signal-to-noise ratio
SSK	space shift keying
STBC	space-time block code
STBC-SM	space-time block coded spatial modulation
TCM	trellis coded modulation
TCSM	trellis coded spatial modulation
V2V	vehicle-to-vehicle
V-BLAST	vertical-bell layered space-time

Chapter 1

Introduction

The proliferation of wireless communication systems such as vehicle-to-vehicle (V2V) communication [1] and wireless high definition (HD) television have fuelled research into MIMO technology. In recent years, MIMO has been considered as one of the core techniques for improving data throughput, link reliability and spectral efficiency [2-4]. MIMO techniques can be divided into two main categories, namely spatial diversity and spatial multiplexing schemes. Spatial diversity techniques [5, 6] improve link reliability by transmitting multiple redundant copies of data to a receiver over independent channels. Alamouti's scheme [6] is a popular transmit diversity technique, which uses a pair of transmit antennas to achieve full transmit diversity. However, diversity gains are traded off by low spectral efficiency, which remains unchanged when compared to a single-input multiple-output (SIMO) system [7].

Spatial multiplexing schemes such as vertical-bell layered space-time (V-BLAST) architecture [8] divide the input data stream into several sub-streams. Each sub-stream is then encoded independently and transmitted in parallel via a specific antenna, thereby increasing capacity. Research efforts have shown that spatial multiplexing techniques are promising candidates for next generation communication systems, since they are able to reach capacities near the Shannon limit [9]. However, spatial multiplexing schemes experience several limitations which reduce their practicality. For example, inter-channel interference (ICI) due to the coupling of multiple symbols in space and time, the need for inter-antenna synchronization (IAS) to ensure the simultaneous transmission of data and high complexity ML detection algorithms [10,11].

SM is a recent MIMO technique proposed by Mesleh *et al*. in [12, 13], which is not prone to the aforementioned spatial multiplexing limitations. The SM scheme encodes data into two information bearing units: an M-QAM/M-ary phase shift keying (M-PSK) symbol and transmit antenna index. The modulated symbol is then transmitted over a wireless channel by a single antenna as specified by the transmit antenna index. In SM, only one antenna is active during transmission, hence ICI and the need for IAS are completely avoided. At the receiver, a maximal-ratio receiver combining (MRRC) based SM detector is used to estimate

both transmit antenna index and modulated symbol. It was shown in [12] that for the same spectral efficiency SM can achieve similar performance to V-BLAST, while maintaining a low complexity detection algorithm. However, Jeganathan *et al*. demonstrated in [14] that the original MRRC SM detector is sub-optimal and therefore proposed an ML based optimal SM detection scheme.

1.1 Recent Work

An upsurge of research interest in SM has led to the development of several novel schemes. Relevant examples to mention are:

- Space shift keying (SSK) modulation in [15] can be considered as a special instance of SM, since only the transmit antenna indices carry information. The SSK scheme eliminated the use of conventional modulation techniques, which reduced receiver complexity as compared to SM. Furthermore, this decrease in receiver complexity was attained without sacrificing performance gains. Similar to SM, SSK schemes work only for a number of transmit antennas which are a power of two. In cases where the transmit antenna constraint cannot be met, the generalized SSK (GSSK) scheme [16] provides a viable solution. In [16], GSSK used a combination of antenna indices to transmit information, which may be applied to any antenna configuration. However, the flexibility of GSSK is traded off by reduced performance as compared to SSK [16].

- Fractional bit encoded spatial modulation (FBE-SM) in [17], which is a more versatile SM scheme based on the theory of modulus conversion. The FBE-SM approach allowed the transmitter to function with an arbitrary number of antennas. As a result, this scheme is well suited to compact mobile devices, where space constraints pose limits on the number of transmit antennas. Numerical results have shown that FBE-SM offers flexibility in design and the necessary degrees of freedom for trading-off attainable performance and capacity [17].

- Trellis coded spatial modulation (TCSM) in [18], which applied trellis coded modulation (TCM) to the antenna constellation points of SM. This increased the free distance between antenna constellation points, thus leading to improved performance over spatially correlated channels. The TCSM scheme was analyzed in [19], where

an analytical framework for the performance over correlated fading channels was proposed.

- Soft-output ML detection in [20], where a soft-output ML detector for SM orthogonal frequency division multiplexing (OFDM) systems was introduced and shown to outperform the conventional hard decision based SM detector.

- SM with partial channel state information (CSI) at the receiver in [21], where an SM detector with unknown phase reference at the receiver was developed and analyzed. Monte Carlo simulations were used as a tool to verify the analytical frameworks and investigate the performance of the proposed detector. Results indicated that SM performance was severely degraded when phase information was not available at the receiver. This highlights the fact that accurate channel estimation is required for the efficient operation of SM detectors [21].

- Optical spatial modulation (OSM) in [22], which is an indoor optical wireless communication technique based on SM. The OSM scheme was shown to achieve twice and four times the data rate as compared to conventional on-off keying and pulse-position modulation techniques, respectively [22]. In [23], channel coding was applied to OSM and the BER performance of both hard and soft detectors were determined analytically. Monte Carlo simulation results demonstrated that the application of channel coding techniques can enhance OSM performance by approximately 5dB and 7dB for hard and soft decisions, respectively [23].

- Normalized maximum ratio combining (NMRC) detector in [24], where a low complexity sub-optimal SM detection algorithm for unconstrained channels was proposed. In addition, an antenna index (AI) list based detector was also introduced in [24]. Monte Carlo simulation results and corresponding analysis indicated that the AI list based scheme can achieve near optimal performance and reduced complexity when compared to the optimal SM detector. However, the AI list based detector can only operate efficiently for list sizes equal to half the number of transmit antennas. This resulted in a 40% increase in complexity as compared to the NMRC scheme [24].

- Space-time block coded spatial modulation (STBC-SM) in [25], which combined SM and STBC in order to exploit the transmit diversity potential of MIMO channels. The proposed scheme was analyzed in [25], where a closed form expression for the average BER was derived. Monte Carlo simulations results were used to support analytical frameworks and also demonstrated the performance advantages of STBC-SM over SM. Results indicated that STBC-SM offers performance enhancements of 3dB-5dB (depending on the spectral efficiency) over conventional SM [25]. It must be highlighted that a similar scheme termed Alamouti coded spatial modulation is proposed in this dissertation. However, both schemes have been developed independently based on the different paradigms employed. This can be further reiterated on the basis that [25] had not been published at the time of submitting this dissertation.

1.2 Motivation and Contributions

The optimal SM detector is analyzed in [14], where the average BER is evaluated in closed form. However, the theoretical performance bound [14, Eq. (8)] is constrained to use with real constellation SM configurations. To the best of the author's knowledge, there have been no publications to date reporting on the theoretical BER of M-QAM spatial modulation with optimal detection (SM-OD). The first contribution of this dissertation is to derive an analytical expression to quantify the average BER of M-QAM SM-OD over i.i.d Rayleigh flat fading channels. Monte Carlo simulation results demonstrate that the derived lower bounds closely predict BER performance in the high SNR region.

The analysis in [14] reveals that both optimal and sub-optimal SM detectors have comparable complexity. However, this condition is only valid for low order $(M \leq 4)$ M-QAM SM configurations. It will be shown subsequently that for high order $(M \geq 16)$ M-QAM SM configurations, M-QAM SM-OD increases receiver complexity by approximately 125% as compared to the sub-optimal SM detector. Therefore, the second contribution of this dissertation is to present a novel SM detection scheme, termed MS detection. The proposed detector aims at achieving optimal performance while maintaining low receiver complexity.

Conventional SM proposals are unable to exploit the transmit diversity provided by the MIMO channel. The third contribution of this dissertation is to introduce a performance

enhanced SM technique, termed Alamouti coded spatial modulation (ACSM). The proposed scheme combines SM with Alamouti STBC, thereby improving the diversity aspect and overall system performance of conventional SM. In order to support our results, a closed form expression for the average BER of real constellation ACSM over i.i.d Rayleigh flat fading channels is derived. The analytical frameworks are validated by Monte Carlo simulation results, which show that the derived upper bounds are increasingly tight in the high SNR region.

1.3 Organization of Dissertation

The remainder of the dissertation is organized as follows:

Chapter 2 provides a brief overview of MIMO systems. Initially, the MIMO system model is introduced followed by a detailed description of the Rayleigh channel model. Several MIMO techniques are also discussed, namely MRRC, Alamouti STBC and SM.

Chapter 3 presents an analytical approach to the BER analysis of M-QAM SM-OD in i.i.d Rayleigh flat fading channels. Thereafter, analytical frameworks are verified through Monte Carlo simulation results.

Chapter 4 introduces the MS detection scheme and provides a detailed description of the two stage detection process. The claimed advantages of MS detection are then substantiated via performance and complexity comparisons with existing SM detectors.

Chapter 5 presents the ACSM technique, including a comprehensive discussion on the transmission and detection mechanisms. An asymptotic performance bound for real constellation ACSM is then derived and its accuracy demonstrated by simulation. This is followed by a performance and complexity comparison between ACSM, Alamouti STBC and SM-OD.

Chapter 6 concludes the dissertation and discusses possible future research directions.

The work is this dissertation has been presented in the following publications:

N. R Naidoo, H. Xu and T. Quazi, "Spatial modulation: Optimal detector asymptotic performance and multiple-stage detection," [Accepted for publication in the *IET Communications Journal*]. The subject matter of this paper is covered in Chapters 3 and 4 of the dissertation.

N. R Naidoo and H. Xu, “Alamouti coded spatial modulation,” [Prepared for submission to the *IET Communications Journal*]. The subject matter of this paper is covered in Chapter 5 of the dissertation.

Chapter 2

Background

The purpose of this chapter is to provide a detailed description of the channel model and MIMO techniques used in this dissertation.

This chapter is outlined as follows: Section 2.1 presents the general MIMO system model and Section 2.2 describes the Rayleigh channel model. Sections 2.3 and 2.4 discuss MRRC and Alamouti STBC techniques, respectively. Finally, the SM scheme is introduced in Section 2.5.

2.1 MIMO System Model

A general MIMO system comprising N_t transmit and N_r receive antennas is shown in Figure 2-1.

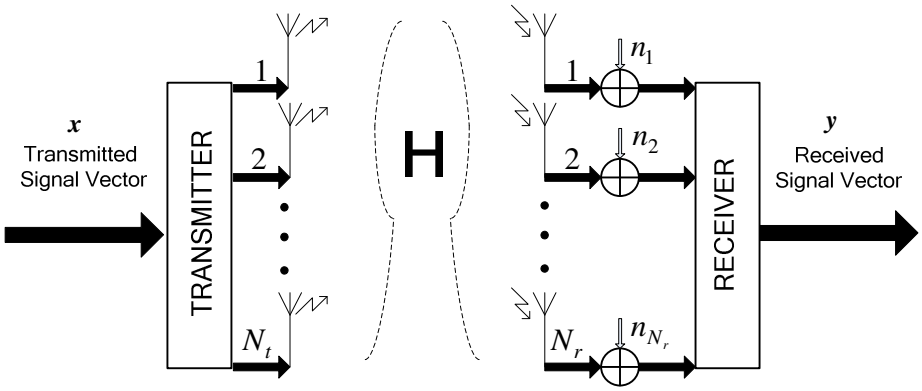

Figure 2-1 MIMO System Comprising N_t Transmit and N_r Receive Antennas

There exists a multipath wireless channel $\boldsymbol{H}(t)$ between the transmitter and receiver. This channel can be represented as follows:

$$\boldsymbol{H}(t) = \begin{bmatrix} \boldsymbol{h}_1(t) & \boldsymbol{h}_2(t) & \boldsymbol{h}_j(t) & \dots & \boldsymbol{h}_{N_t}(t) \end{bmatrix} \tag{2-1}$$

where $j \epsilon [1: N_t]$ and $\boldsymbol{h}_j(t) = \begin{bmatrix} h_{1,j}(t) & h_{2,j}(t) & \dots & h_{N_r,j}(t) \end{bmatrix}^T$ represents the channel path gains between the j^{th} transmit antenna and its corresponding receive antennas at time t.

Consider the N_t dimensional signal vector $\boldsymbol{x}(t) = \left[x_1(t)\ x_2(t) \ldots x_{N_t}(t)\right]^T$, where $x_{N_t}(t)$ corresponds to the symbol transmitted via the ${N_t}^{th}$ transmit antenna. The signal vector is simultaneously transmitted over the MIMO channel $\boldsymbol{H}(t)$, experiencing N_r dimensional additive white Gaussian noise (AWGN) $\boldsymbol{n}(t) = \left[n_1(t)\, n_2(t) \ldots . n_{N_r}(t)\right]^T$. The received signal vector at a discrete time t is given by:

$$\boldsymbol{y}(t) = \sqrt{p(t)}\boldsymbol{H}(t) * \boldsymbol{x}(t) + \boldsymbol{n}(t) \tag{2-2}$$

where $p(t)$ is the average SNR at each receive antenna and $\boldsymbol{y}(t) = \left[y_1(t)\, y_2(t) \ldots y_{N_r}(t)\right]^T$ is the received signal vector. Note that the AWGN vector $\boldsymbol{n}$ has i.i.d entries according to the complex Gaussian distribution $\mathcal{CN}(0,1)$.

In this dissertation, the channel $\boldsymbol{H}(t)$ is assumed to be frequency non-selective. This implies that the signal bandwidth is less than the coherence bandwidth of the channel. As a result, the channel gain is constant over the bandwidth of the transmitted signal and the convolution operation in (2-2) reduces to a simple multiplication.

$$\boldsymbol{y} = \sqrt{p}\boldsymbol{H}\boldsymbol{x} + \boldsymbol{n} \tag{2-3}$$

where the time index in (2-3) has been dropped to simplify notation.

2.2 Wireless Channel Model

The wireless channel is characterized by two fundamental impairments [26]: large-scale and small-scale fading.

- **Large-scale fading** decreases signal power over time. This type of fading is due to the path loss (distance dependant) of a signal and the presence of large objects in the signal path.

- **Small-scale fading** is caused by multipath signal propagation. This type of fading occurs when multiple versions of a signal add destructively, resulting in a distorted signal.

This dissertation considers the effects of small scale fading, where the channel under consideration is flat or frequency non-selective. The classical Rayleigh flat fading channel model is presented next.

2.2.1 Rayleigh Fading

Rayleigh fading is usually encountered in urban areas, which have a large number of reflectors and no line-of-sight (LOS) path between the transmitter and receiver. The fading channel is modelled by a complex multiplicative distortion matrix $\boldsymbol{H}$ as shown in (2-1). The matrix $\boldsymbol{H}$ consists of i.i.d complex Gaussian random variable (GRV) entries:

$$\alpha = \alpha_1 + i\alpha_2 \tag{2-4}$$

where α is distributed according to $\mathcal{CN}(\mu, \sigma^2)$ with $\mu = 0$ and $\sigma^2 = 1$.

Thus, the fading amplitude $A = \sqrt{{\alpha_1}^2 + {\alpha_2}^2}$ is Rayleigh distributed according to [27, Eq. (3.32)]:

$$f(A) = \frac{A}{\sigma^2} exp\left(\frac{-A^2}{2\sigma^2}\right) \quad A \geq 0 \tag{2-5}$$

The fading phase is given by [27]:

$$\emptyset = arctan(\alpha_2/\alpha_1) \tag{2-6}$$

where $\emptyset$ is uniformly distributed from 0 to 2π.

2.3 Receive Diversity: Maximal-Ratio Receiver Combining

Receive diversity techniques, MRRC for example, utilize multiple antennas at the receiver to obtain independent replicas of the transmitted signal. These replicas are then combined at the receiver in order to increase the SNR, thereby improving link reliability. Receive diversity techniques are not practical for use in downlink (base station to mobile unit), since the multiple antennas significantly increase the complexity and cost of mobile units. Hence, these techniques are almost exclusively applied at the base stations to improve uplink (mobile unit to base station) performance [6].

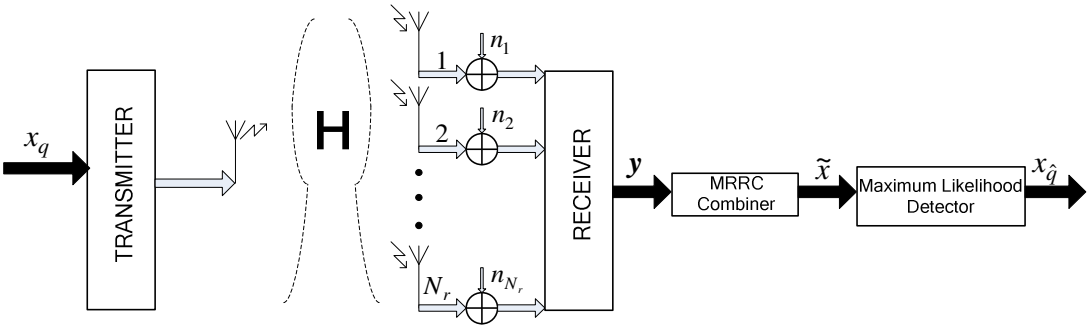

Figure 2-2 MRRC System Comprising 1 Transmit and N_r Receive Antennas

Figure 2-2 shows the system model for an N_r branch MRRC scheme. In a given time slot, symbol x_q is transmitted over the wireless channel via a single antenna. The received signal vector is given by:

$$\boldsymbol{y} = \sqrt{p}\boldsymbol{H}x_q + \boldsymbol{n} \tag{2-7}$$

where $\boldsymbol{y} = \left[y_1\, y_2 \ldots y_{N_r} \right]^T$ is the received signal vector, p is the average SNR at each receive antenna, $\boldsymbol{H} = \left[h_{1,1}\, h_{2,1} \ldots h_{N_r,1}\right]^T$ refers to the N_r dimensional channel matrix, x_q corresponds to the q^{th} symbol from an M-ary constellation and $\boldsymbol{n} = \left[n_1\, n_2 \ldots\, n_{N_r}\right]^T$ is the N_r dimensional AWGN vector.

Assuming perfect CSI at the receiver, the MRRC scheme constructs the following signal [6, Eq. (5)]:

$$\tilde{x} = \sum_{k=1}^{N_r} h_{k,1}^{*}\, y_k \tag{2-8}$$

The ML detector then obtains a symbol estimate based on the combined signal (2-8) [6, Eq. (6)]:

$$x_{\hat{q}} = \underset{q}{argmin}\, \sqrt{p}\left\|\boldsymbol{H}x_q\right\|_F^2 - 2Re\{\tilde{x}x_q^*\} \tag{2-9}$$

where $x_{\hat{q}}$ represents the estimated symbol and $q\epsilon[1{:}\,M]$.

2.4 Transmit Diversity: Alamouti Space-Time Block Coding

Transmit diversity techniques such as STBC [5,6] mitigate small-scale fading impairments by transmitting multiple redundant copies of data to a receiver over independent channels. STBC schemes are well suited for downlink transmission as they require the addition of equipment to base stations rather than remote units. Alamouti's scheme [6] is a popular STBC technique, which utilizes a pair of transmit antennas to achieve full transmit diversity. This scheme is orthogonal by design and is therefore not prone to the adverse effects of ICI. However, IAS is required to ensure the simultaneous transmission of data from both antennas. The Alamouti code is proposed specifically for a two transmit $(N_t = 2)$ multiple receive (N_r) antenna architecture as shown in Figure 2-3. The Alamouti STBC scheme is defined by three functions: encoding of data symbols; combining at the receiver and ML detection [6]. In what follows, each function will be described in detail.

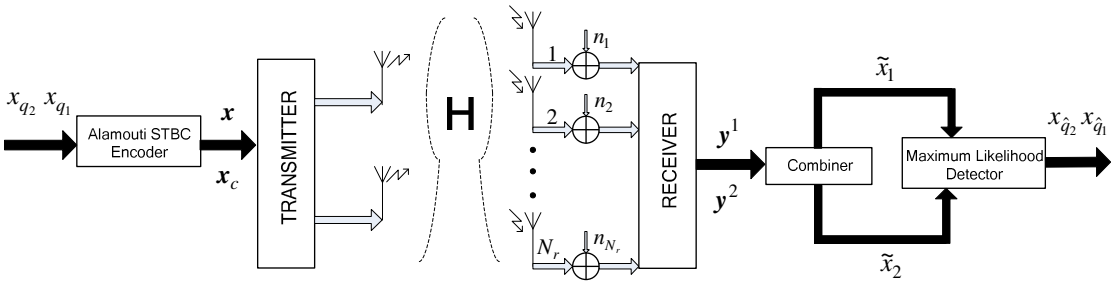

Figure 2-3 Alamouti STBC System Comprising 2 Transmit and N_r Receive Antennas

2.4.1 Encoding

Consider the transmission sequence $[x_{q_1}\ x_{q_2}]$, where x_{q_1} and x_{q_2} represent the ${q_1}^{th}$ and ${q_2}^{th}$ symbols from an M-ary constellation, respectively. In a given time slot there will be a simultaneous transmission of two symbols by two transmit antennas. In the first time slot, x_{q_1} and x_{q_2} are transmitted via the first and second transmit antennas, respectively. During the second time slot, $-x_{q_2}^*$ and $x_{q_1}^*$ are transmitted by the first and second transmit antennas, respectively. The space-time encoded transmission sequence is shown in Table 2.1.

Table 2.1 Space-Time Encoded Transmission Sequence

	Transmit Antenna 1	Transmit Antenna 2
First Time Slot	x_{q_1}	x_{q_2}
Second Time Slot	$-x_{q_2}^*$	$x_{q_1}^*$

Assuming constant fading coefficients over two consecutive time slots, the received signal vectors in the first and second time slots are as follows:

First time slot:

$$\boldsymbol{y}^1 = \sqrt{p}\boldsymbol{H}\boldsymbol{x} + \boldsymbol{n}^1 \tag{2-10}$$

where $\boldsymbol{y}^1 = \left[y_1^1 \;\; y_n^1 \ldots y_{N_r}^1\right]^T$ denotes the received signal vector in the first time slot, p is the average SNR at each receive antenna, $\boldsymbol{H} = \begin{bmatrix} h_{1,1} & \ldots & h_{2,1} & h_{N_r,1} \\ h_{1,2} & \ldots & h_{2,2} & h_{N_r,2} \end{bmatrix}^T$ refers to the $N_r \times 2$ dimensional channel matrix, $\boldsymbol{x} = \left[x_{q1}\, x_{q2}\right]^T$, $\boldsymbol{n}^1 = \left[n_1^1 \;\; n_2^1 \ldots n_{N_r}^1\right]^T$ is the N_r dimensional AWGN vector and $E[\boldsymbol{x}^H\boldsymbol{x}] = 1$ to ensure unity transmit power.

Second time slot:

$$\boldsymbol{y}^2 = \sqrt{p}\boldsymbol{H}\boldsymbol{x}_c + \boldsymbol{n}^2 \tag{2-11}$$

where $\boldsymbol{y}^2 = \left[y_1^2 \;\; y_2^2 \ldots y_{N_r}^2\right]^T$ denotes the received signal vector in the second time slot, $\boldsymbol{x}_c = \left[-x_{q2}{}^*\; x_{q1}{}^*\right]^T$, $\boldsymbol{n}^2 = \left[n_1^2 \;\; n_2^2 \ldots n_{N_r}^2\right]^T$ is the N_r dimensional AWGN vector and $E[\boldsymbol{x}_c{}^H\boldsymbol{x}_c] = 1$ to ensure unity transmit power.

In Alamouti STBC, two symbols are transmitted per time slot. However, two time slots are still required for the transmission of both symbols, hence Alamouti STBC does not affect the data rate.

2.4.2 Combination and Detection

The orthogonality of Alamouti STBC permits the decoupling of symbols during the combination and detection processes. Assuming perfect CSI at the receiver, the combiner forms the following two signals [6, Eq. (15)]:

$$\tilde{x}_1 = \sum_{k=1}^{N_r} h_{k,1}^{*}\, y_k^1 + h_{k,2}\, y_k^{2^*} \tag{2-12}$$

$$\tilde{x}_2 = \sum_{k=1}^{N_r} h_{k,2}^{*}\, y_k^1 - h_{k,1}\, y_k^{2^*} \tag{2-13}$$

Finally, the combined signals (2-12) and (2-13) are input to the ML detector which obtains symbol estimates $x_{\hat{q}_1}$ and $x_{\hat{q}_2}$ by computing [6, Eq. (19)]:

$$x_{\hat{q}_1} = \underset{q_1}{argmin}\ \sqrt{p}\left\|\boldsymbol{H}x_{q_1}\right\|_F^2 - 2Re\{\tilde{x}_1 x_{q_1}^{*}\} \tag{2-14}$$

$$x_{\hat{q}_2} = \underset{q_2}{argmin}\ \sqrt{p}\left\|\boldsymbol{H}x_{q_2}\right\|_F^2 - 2Re\{\tilde{x}_2 x_{q_2}^{*}\} \tag{2-15}$$

where $q_1 \in [1{:}\,M]$ and $q_2 \in [1{:}\,M]$.

2.5 Spatial Modulation

Spatial modulation is a recent MIMO technique proposed for high speed uplink transmission in next generation networks [12]. SM schemes are unique as they encode data in both the spatial (transmit antenna indices) and signal domains (digital modulation scheme). In SM, a sequence of bits are mapped to an M-QAM/M-PSK symbol and transmit antenna index. The modulated symbol is then transmitted over the wireless channel via a single antenna as specified by the transmit antenna index. Hence, SM schemes avoid the ICI and IAS issues inherent to MIMO systems [12]. At the receiver, the SM detector estimates the active transmit antenna index and modulated symbol in order to recover the original bit sequence. In the following, SM transmission and detection processes are discussed in detail.

2.5.1 Transmission

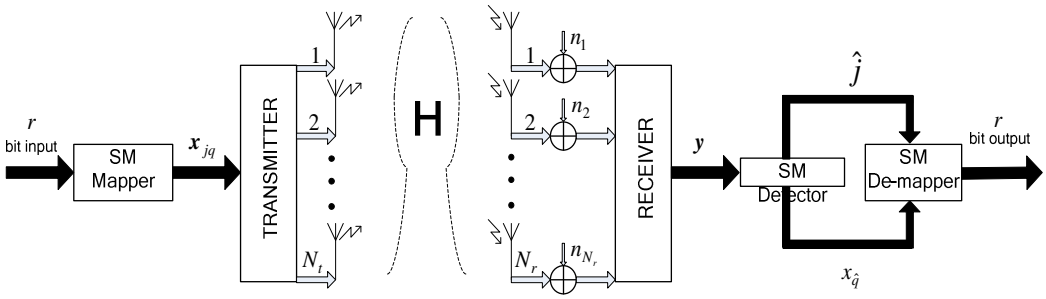

Figure 2-4 SM System Comprising N_t Transmit and N_r Receive Antennas

The $N_t \times N_r$ M-QAM / M-PSK SM system model is shown in Figure 2-4. Initially, the SM mapper assigns a random r bit binary input to a modulated symbol x_q and a unique transmit antenna index j. The assignment of j and x_q are defined by the SM mapping table, which is assumed to be known at both transmitter and receiver. A sample SM mapping table for 3bits/sec/Hz SM transmission is shown in Figure 2 of [12]. In general, the number of bits that can be transmitted using SM is given by [12]:

$$r = log_2(MN_t) \tag{2-16}$$

where M denotes the order of digital modulation scheme used.

It is clearly shown in (2-16) that SM schemes improve the overall spectral efficiency by the base two logarithm of the number of transmit antennas and work only for a number of transmit antennas which are power of two [28]. In SM, the number of transmit antennas or digital modulation scheme can be adjusted in order to achieve a desired transmission rate. For example, a transmission rate of 4 bps can be achieved by the 4×4 4-QAM SM configuration. Alternatively, the same transmission rate can also be achieved by the 2×4 8-QAM SM configuration.

The SM mapper output can be expressed as [14]:

$$\boldsymbol{x}_{jq} = \begin{bmatrix} 0 & 0 \dots x_q \dots 0 \end{bmatrix}^T \quad \begin{matrix} j^{th}\ position \\ \downarrow \\ \uparrow \quad\quad \uparrow \\ 1^{st} position \quad\quad N_t{}^{th}\ position \end{matrix} \tag{2-17}$$

where $\boldsymbol{x}_{jq}$ is an N_t dimensional signal vector, x_q denotes the q^{th} symbol from an M-ary constellation with $q\epsilon[1:M]$, $j\epsilon[1:N_t]$ and $E\left[\left|x_q\right|^2\right] = 1$. Note that the signal vector (2-17) has a single non-zero entry x_q at the j^{th} position corresponding to the active transmit antenna index and $N_t - 1$ zero entries corresponding to the dormant transmit antenna indices.

After the mapping process, signal vector $\boldsymbol{x}_{jq}$ is transmitted over the $N_r \times N_t$ dimensional MIMO channel $\boldsymbol{H}$, experiencing N_r dimensional AWGN $\boldsymbol{n} = \left[n_1, n_2 \dots . n_{N_r}\right]^T$**.** The received signal vector is given by [14]:

$$\boldsymbol{y} = \sqrt{p}\boldsymbol{H}\boldsymbol{x}_{jq} + \boldsymbol{n} \tag{2-18}$$

where p denotes the average SNR at each receive antenna and $\boldsymbol{y} = \left[\, y_1\, y_2 \dots y_{N_r}\right]^T$ represents the received signal vector.

Assuming transmission from the j^{th} transmit antenna, the received signal vector can also be represented by [14, Eq. (1)]:

$$\boldsymbol{y} = \sqrt{p}\boldsymbol{h}_j\boldsymbol{x}_q + \boldsymbol{n} \tag{2-19}$$

where $\boldsymbol{h}_j$ denotes the j^{th} column of $\boldsymbol{H}$**.**

At the receiver, the SM detector obtains estimates of the transmit antenna index and modulated symbol. These estimates are then input to the SM de-mapper, which uses the SM mapping table to perform a reverse mapping process in order to recover an estimate of the original r bit binary input. Note that the SM detection process assumes perfect CSI at the receiver.

2.5.2 Sub-Optimal Detection

The sub-optimal SM detector decouples the transmit antenna and symbol estimation processes. The transmit antenna index is estimated first followed by symbol estimation. In general, these two estimation processes are interdependent and their subsequent decoupling during detection leads to reduced performance. The sub-optimal detector is based on MRRC and is applied to the received signal vector as follows [12, Eq. (4)]:

$$z_j = \frac{\boldsymbol{h}_j{}^H \boldsymbol{y}}{\|\boldsymbol{h}_j\|_F^2} \tag{2-20}$$

where $j \in [1: N_t]$ and $\|\boldsymbol{h}_j\|_F^2 = 1$ for constrained channels [14].

The active transmit antenna index is estimated by computing [12, Eq. (6)]:

$$\hat{j} = \underset{j}{argmax} |z_j| \tag{2-21}$$

where $\hat{j}$ represents the estimated transmit antenna index.

Assuming perfect transmit antenna estimation, the combined symbol based on MRRC is given by:

$$\tilde{x} = z_{\hat{j}} = \boldsymbol{h}_{\hat{j}}{}^H \boldsymbol{y} \tag{2-22}$$

The ML criterion is then applied in order to obtain a symbol estimate [6, Eq. (6)]:

$$x_{\hat{q}} = \underset{q}{argmin} \quad \sqrt{p}\|\boldsymbol{h}_j x_q\|_F^2 - 2Re\{\tilde{x}\, x_q^*\} \tag{2-23}$$

where $x_{\hat{q}}$ represents the modulated symbol estimate and $q \in [1: M]$.

In [14] Jeganathan *et al*. showed that the sub-optimal SM detector is only applicable in constrained channel conditions, where a constrained channel is obtained by normalizing the channel prior to transmission such that $\|\boldsymbol{h}_j\|_F^2 = c$ for all j and constant c. Since the sub-optimal detector only operates under some impractical channel assumptions, a modified version of this scheme is suggested in this dissertation. The modified sub-optimal detection rules can be applied in conventional channel conditions as follows:

$$z_j = \frac{\boldsymbol{h}_j{}^H \boldsymbol{y}}{\|\boldsymbol{h}_j\|_F} \tag{2-24}$$

where $j \in [1: N_t]$.

Similar to (2-21), the transmit antenna index is estimated by:

$$\hat{j} = \underset{j}{argmax} |z_j| \tag{2-25}$$

where $\hat{j}$ represents the estimated transmit antenna index.

Assuming perfect transmit antenna estimation, the combined symbol based on MRRC is given by:

$$\tilde{x} = \|\boldsymbol{h}_{\hat{j}}\|_F z_{\hat{j}} = \boldsymbol{h}_{\hat{j}}{}^H \boldsymbol{y} \tag{2-26}$$

Finally, the symbol estimate $x_{\hat{q}}$ is obtained by computing (2-23).

2.5.3 Optimal Detection

The ML based SM detector achieves optimal performance by executing a joint detection of transmit antenna index and symbol. The optimal detection rule can be applied as follows [14, Eq. (4)]:

$$\begin{aligned} [\hat{j}, x_{\hat{q}}] &= \underset{j,q}{argmax} \quad p_Y(\boldsymbol{y}|\boldsymbol{x}_{jq}, \boldsymbol{H}) \\ &= \underset{j,q}{argmin} \quad \left[\sqrt{p}\|\boldsymbol{g}_{jq}\|_F^2 - 2Re\{\boldsymbol{y}^H \boldsymbol{g}_{jq}\}\right] \end{aligned} \tag{2-27}$$

where $\boldsymbol{g}_{jq} = \boldsymbol{h}_j x_q, j \epsilon [1: N_t]$ and $q \epsilon [1: M]$. $\hat{j}$ and $x_{\hat{q}}$ represent the estimated transmit antenna index and symbol based on ML, respectively and $p_Y(\boldsymbol{y}|\boldsymbol{x}_{jq}, \boldsymbol{H}) = \pi^{-Nr} exp\left(-\|\boldsymbol{y} - \sqrt{p}\boldsymbol{H}\boldsymbol{x}_{jq}\|_F^2\right)$ is the probability density function (PDF) of the received signal vector $\boldsymbol{y}$ conditioned on both $\boldsymbol{x}_{jq}$ and $\boldsymbol{H}$.

2.5.4 Features

The key features of SM can be summarized by the following points [28]:

- **ICI and IAS avoidance**: A single antenna is active during transmission. As a result, SM schemes do not require IAS and are not prone to ICI.
- **Receive diversity**: Multiple antennas are used at the receiver in order to obtain receive diversity gains.
- **Enhanced spectral efficiency**: Data is encoded in the transmit antenna index, thereby increasing spectral efficiency by the base two logarithm of the total number of transmit antennas.
- **Restricted number of transmit antennas**: The SM scheme functions only for a number of transmit antennas which are a power of two.

Chapter 3

Asymptotic Performance Analysis of M-QAM Spatial Modulation with Optimal Detection

The ML based optimal SM detector was introduced in Section 2.5.3. In [14] Jeganathan *et al*. analyzed the optimal detector performance by deriving a closed form expression for the average BER over fading channels. However, the theoretical performance bound [14, Eq. (8)] is inadequate since it can only predict the performance of binary phase shift keying (BPSK) SM configurations. The ever increasing need for high rate data transmission cannot be met using a low rate digital modulation technique like BPSK in conjunction with SM. In order to increase the data rate it is necessary to combine SM with a more spectrally efficient technique such as M-QAM. To date, there has been no literature reporting on the theoretical performance of an M-QAM SM-OD scheme in fading channel conditions. The aim of this chapter is to derive an analytical expression to quantify the average BER of M-QAM SM-OD over i.i.d Rayleigh flat fading channels.

This chapter is outlined as follows: Section 3.1 presents an asymptotic performance bound for the overall BER of M-QAM SM-OD. Sections 3.2 and 3.3 consider the BER of the symbol and transmit antenna estimation processes, respectively. Simulation results are then presented and discussed in Section 3.4 and a chapter summary is given in Section 3.5.

3.1 Analytical BER of Spatial Modulation

The SM detector is responsible for the estimation of two quantities: the active transmit antenna index and transmitted symbol. As a result, SM performance depends on the error rates of these two processes. The subsequent analysis follows the same approach as in [29], where independent transmit antenna index and symbol estimation processes are assumed. Let P_a denote the bit error probability of transmit antenna index estimation given that the symbol is perfectly detected and P_d be the bit error probability of symbol estimation given that the transmit antenna index is perfectly detected. The overall probability of bit error is then bounded by:

$$P_e \geq 1 - P_c = P_a + P_d - P_a P_d \tag{3-1}$$

where $P_c = (1 - P_a)(1 - P_d)$ is the probability of correct SM bits.

In general, it is incorrect to assume independent estimation processes, since the optimal SM detector performs a joint detection of transmit antenna index and symbol. The assumption of independent estimation processes represents an ideal scenario and therefore (3-1) corresponds to the best performance (lower bound) achievable by M-QAM SM-OD. In what follows, the BER of each estimation process is considered separately.

3.2 Analytical BER of Symbol Estimation

In SM, only one antenna is active during transmission. Therefore, at any instant the $N_t \times N_r$ SM model may be viewed as a $1 \times N_r$ SIMO configuration. Assuming perfect transmit antenna detection, the SM detector applies the ML criterion for symbol detection as follows:

$$x_{\hat{q}} = \underset{q}{argmin} \quad \sqrt{p}\left\|\boldsymbol{g}_{jq}\right\|_F^2 - 2Re\{\boldsymbol{y}^H \boldsymbol{g}_{jq}\} \tag{3-2}$$

where $x_{\hat{q}}$ represents the estimated symbol based on ML, p is the average SNR at each receive antenna, $\boldsymbol{g}_{jq} = \boldsymbol{h}_j x_q$, $\boldsymbol{h}_j$ denotes the j^{th} column of channel matrix $\boldsymbol{H}$, x_q refers to the q^{th} symbol from an M-QAM constellation, $q \epsilon [1: M]$ and $\boldsymbol{y}$ is the received signal vector.

In [6] Alamouti shows that (3-2) is equivalent to an N_r branch MRRC of the received signal followed by a regular symbol-by-symbol detection. The average symbol error rate (SER) of square M-QAM with MRRC reception over Rayleigh fading channels given by [30, Eq. (15)]:

$$SER(p) = \frac{a}{c}\left\{\frac{1}{2}\left(\frac{2}{bp+2}\right)^{N_r} - \frac{a}{2}\left(\frac{1}{bp+1}\right)^{N_r} + (1-a)\sum_{i=1}^{c-1}\left(\frac{S_i}{bp+S_i}\right)^{N_r} + \sum_{i=c}^{2c-1}\left(\frac{S_i}{bp+S_i}\right)^{N_r}\right\} \tag{3-3}$$

where $a = \left(1 - \frac{1}{\sqrt{M}}\right)$, $b = \frac{3}{M-1}$, $m = log_2(M)$, $S_i = 2sin^2\theta_i$, $\theta_i = \frac{i\pi}{4n}$, N_r is the number of receive antennas and c is the number of summations. It is shown in [31] that applying $c >$ 10 results in a 0.0015 dB, 0.0025 dB and 0.0029 dB difference between the simulated and theoretical SER for the 4, 16 and 64-QAM configurations, respectively.

P_d is then derived from the approximate relationship [32] as follows:

$$P_d \cong \frac{SER}{m} \tag{3-4}$$

where $m = log_2(M)$ is the number of bits per M-QAM symbol.

3.3 Analytical BER of Transmit Antenna Index Estimation

The bit error probability of transmit antenna index estimation is derived using the same approach as in [15]. Given that the transmitted symbol is perfectly detected, the average BER of transmit antenna index estimation is union bounded by [32, pp. 261-262]:

$$P_a \leq E_j\left[\sum_{\hat{j}} N(j,\hat{j})P\left(\boldsymbol{x}_{jq} \to \boldsymbol{x}_{\hat{j}q}\right)\right] = \sum_{j=1}^{N_t}\sum_{q=1}^{M}\sum_{\hat{j}=1}^{N_t}\frac{N(j,\hat{j})P\left(\boldsymbol{x}_{jq} \to \boldsymbol{x}_{\hat{j}q}\right)}{N_t M} \tag{3-5}$$

where $P\left(\boldsymbol{x}_{jq} \to \boldsymbol{x}_{\hat{j}q}\right)$ denotes the pairwise error probability (PEP) of choosing signal vector $\boldsymbol{x}_{\hat{j}q}$ given that $\boldsymbol{x}_{jq}$ was transmitted and $N(j,\hat{j})$ is the number of bits in error between transmit antenna index j and estimated transmit antenna index $\hat{j}$.

The PEP conditioned on channel matrix $\boldsymbol{H}$ is given by (refer to Appendix A for derivation):

$$P\left(\boldsymbol{x}_{jq} \to \boldsymbol{x}_{\hat{j}q}|\boldsymbol{H}\right) = P\left(\left\|\boldsymbol{y} - \sqrt{p}\boldsymbol{h}_{\hat{j}}x_q\right\|_F < \left\|\boldsymbol{y} - \sqrt{p}\boldsymbol{h}_j x_q\right\|_F \,\middle|\, \boldsymbol{H}\right) = Q\left(\sqrt{k}\right) \tag{3-6}$$

where $Q(x) = \int_x^\infty \frac{1}{\sqrt{2\pi}} e^{-t^2/2}\, dt$ and k is defined as [15, Eq. (5)]:

$$k = \frac{p}{2}\left\|\left(\boldsymbol{h}_j x_q - \boldsymbol{h}_{\hat{j}} x_q\right)\right\|_F^2 = \sum_{n=1}^{2N_r}\alpha_n^2 \tag{3-7}$$

where $\alpha_n \sim \mathcal{N}(0, \sigma_\alpha^2)$ with $\sigma_\alpha^2 = \frac{p}{2}\left|x_q\right|^2$.

The random variable k is the summation of $2N_r$ squared i.i.d Gaussian random variables.

Hence, k has a central Chi-square distribution with $2N_r$ degrees of freedom and PDF given by [32, p. 41]:

$$p_k(v) = \frac{v^{N_r-1}e^{-v/2\sigma_\alpha^2}}{(2\sigma_\alpha^2)^{N_r}\Gamma(N_r)} \quad for\ v > 0 \tag{3-8}$$

where $\Gamma(N_r) = \int_0^\infty t^{N_r-1}\, e^{-t}dt$ is the gamma function.

Since k has a known distribution the PEP term in (3-5) can be computed as follows [15, Eq. (6)]:

$$P\left(\boldsymbol{x}_{jq} \to \boldsymbol{x}_{\hat{j}q}\right) = \int_{v=0}^{\infty} Q\left(\sqrt{v}\right) p_k(v)dv \tag{3-9}$$

The closed form solution for (3-9) is given in [33, Eq. (64)]:

$$P\left(\boldsymbol{x}_{jq} \to \boldsymbol{x}_{\hat{j}q}\right) = \mu_\alpha^{N_r} \sum_{w=0}^{N_r-1} \binom{N_r-1+w}{w} [1-\mu_\alpha]^w \tag{3-10}$$

where $\mu_\alpha = \frac{1}{2}\left(1 - \sqrt{\frac{\sigma_\alpha^2}{1+\sigma_\alpha^2}}\right)$.

Finally, substituting (3-10) into (3-5) yields:

$$P_a \leq \sum_{j=1}^{N_t}\sum_{q=1}^{M}\sum_{\hat{j}=1}^{N_t} \frac{N(j,\hat{j})\mu_\alpha^{N_r} \sum_{w=0}^{N_r-1}\binom{N_r-1+w}{w}[1-\mu_\alpha]^w}{N_t M} \tag{3-11}$$

3.4 Analytical and Simulated BER Comparison

The aim of this section is to validate the analytical frameworks developed in Sections 3.1 to 3.3. Monte Carlo simulations are performed over an i.i.d Rayleigh flat fading channel with AWGN, where the average BER is plotted against the average SNR at each receive antenna. The following were assumed during simulation: the channel matrix $\boldsymbol{H}$ and AWGN vector $\boldsymbol{n}$ comprise i.i.d entries distributed according to $\mathcal{CN}(0,1)$; Gray Coded M-QAM constellation;

full channel knowledge at receiver; transmit and receive antennas are separated wide enough to avoid correlation and the total transmit power is the same for all transmissions.

3.4.1 Analytical and Simulated BER of Symbol Estimation

Figure 3-1 shows the analytical and simulated average BER of the symbol estimation process for 4×4 M-QAM SM-OD. The relation in (3-4) assumes that one symbol error is equivalent to one bit error. However, this relation is generally incorrect at low SNR values, where a single symbol error may correspond to multiple bit errors. This explains why the analytical BER underestimates the simulated BER at low SNR values. For high SNR values, the probability of a symbol error with multiple bit errors is negligible. As a result, both analytical and simulated BER show a close match in the high SNR region.

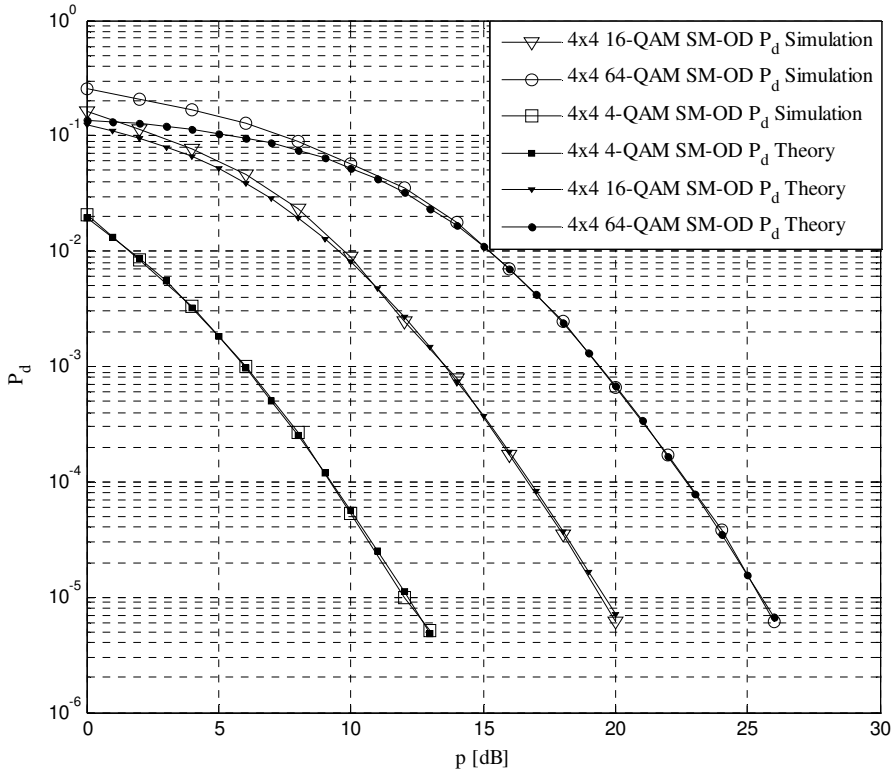

Figure 3-1 4x4 M-QAM SM-OD Analytical and Simulated P_d Comparison

3.4.2 Analytical and Simulated BER of Transmit Antenna Index Estimation

Figure 3-2 shows the analytical and simulated average BER of the transmit antenna estimation process for 4×4 M-QAM SM-OD. As expected, the union bound overestimates the simulated BER at low SNR values and becomes tight in the high SNR region. Therefore, (3-11) does not change the direction of the inequality (3-1) for high values of SNR.

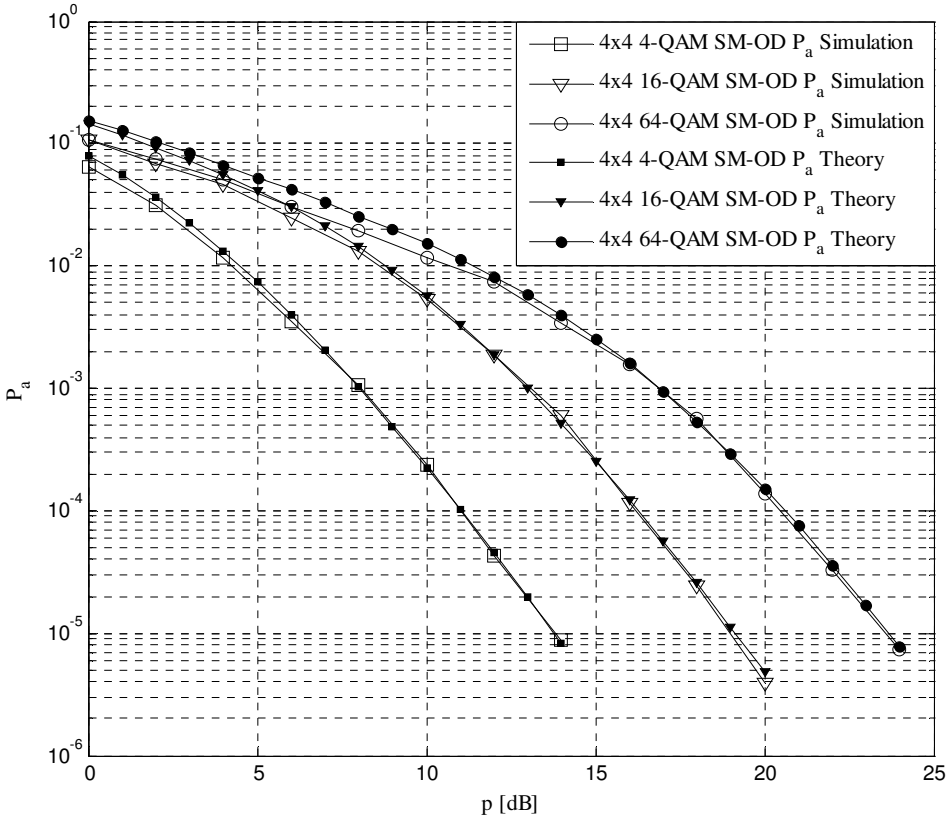

Figure 3-2 4x4 M-QAM SM-OD Analytical and Simulated P_a Comparison

3.4.3 Analytical and Simulated BER of M-QAM Spatial Modulation with Optimal Detection

The analytical and simulated average BER for 2×4 and 4×4 M-QAM SM-OD are shown in Figures 3-3 and 3-4, respectively. The results in Figure 3-3 demonstrate that the theoretical bound closely estimates the BER performance of 2×4 M-QAM SM-OD for the entire range of considered SNR. However, the theoretical bound is observed to be relatively loose for 4×4 4-QAM SM-OD, as shown in Figure 3-4. The reason for this behaviour is that the transmit antenna index error (P_a) dominates over the symbol error (P_d) when the number of transmit antenna bits $(log_2 N_t)$ are greater than or equal to the number of symbol bits $\left(log_2 M\right)$. This hypothesis is supported by the 4×4 4-QAM SM-OD results in Figures 3-1 and 3-2, which reveal that P_a is larger than P_d by approximately an order of magnitude. For example, at an SNR of 10 dB $P_a = 2 \times 10^{-4}$ while $P_d = 4 \times 10^{-5}$. Since P_a dominates, the effects of P_d become negligible and the bound $P_e \geq P_a + P_d - P_a P_d$ can be simplified to $P_e \geq P_a$. Therefore, the analytical lower bound becomes less tight for SM configurations where $log_2 N_t \geq log_2 M$.

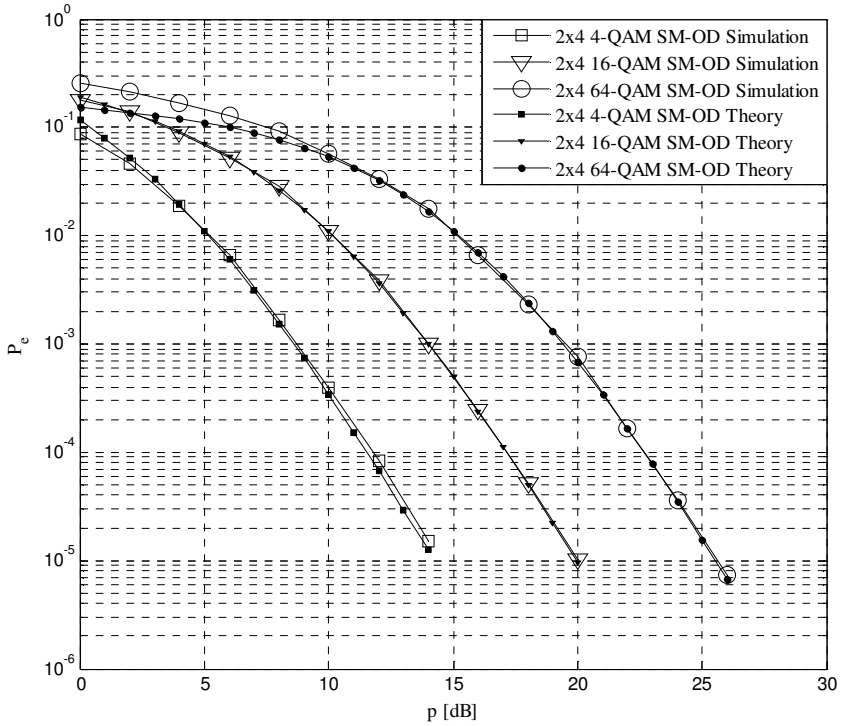

Figure 3-3 2x4 *M*-QAM SM-OD Analytical and Simulated P_e Comparison

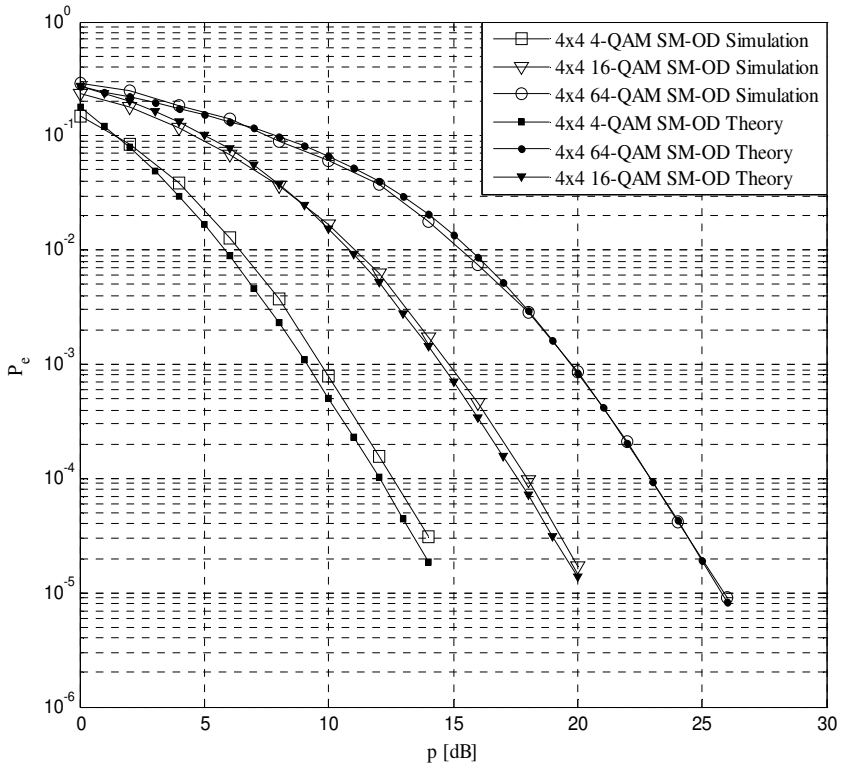

Figure 3-4 4x4 *M*-QAM SM-OD Analytical and Simulated P_e Comparison

3.5 Chapter Summary

A theoretical performance bound to quantify the average BER of M-QAM SM-OD over i.i.d Rayleigh flat fading channels was derived in this chapter. The theoretical bound was shown to be relatively tight, thereby validating analytical frameworks. The next chapter will present a novel SM detection scheme which aims at reducing the high computational complexity inherent to the optimal SM detector, while maintaining equivalent performance.

Chapter 4

Multiple-Stage Detection

The SM scheme encodes data into a transmit antenna index and modulated symbol. As a result, SM detection requires the accurate estimation of both these information bearing units. The optimal SM detector is based on the ML technique, which can become extremely complex with high order modulation schemes and a moderate number of transmit antennas. On the other hand, MRRC based SM detection has low computational complexity but exhibits sub-optimal performance. The limitation of these two SM detectors motivated an investigation into an alternate SM detection scheme, termed MS detection. The proposed detector is a hybrid scheme which combines the operation of both sub-optimal and optimal SM detectors. Therefore, the MS detector inherits the desirable properties of its constituent detectors namely, the low complexity of sub-optimal detection and the high performance of optimal detection.

This chapter is outlined as follows: Section 4.1 presents the MS detection scheme. The detection rules applied in the first and second stages of MS are then given in Sections 4.2 and 4.3, respectively. Section 4.4 shows a performance comparison between MS, sub-optimal and optimal SM detection schemes. Section 4.5 analyzes the various detectors in terms of computational complexity and finally, a chapter summary is given in Section 4.6.

4.1 The Multiple-Stage Detection Process

The optimal SM detector requires a brute force search amongst all possible $(N_t M)$ pairs of transmit antenna index and modulated symbol. As a consequence, the complexity of SM-OD increases rapidly with modulation order M and the number of transmit antennas N_t. One way to decrease the complexity of SM-OD is to reduce the number of inputs to the detector. The MS detection scheme achieves this reduction in detector input by splitting the SM detection process into two stages, as shown in Figure 4-1. The first stage of MS uses the low complexity sub-optimal (MRRC) SM detector to select the N $(N \leq N_t)$ most probable estimates of transmit antenna index, thereby decreasing the number of possible inputs pairs from $N_t M$ to NM. The reduced input set is then sent to the optimal (ML) SM detector in the second stage of MS, where a final estimate of transmit antenna index ($\hat{j}_{MS}$) and modulated

symbol ($x_{\hat{q}_{MS}}$) is obtained. Since the NM input pairs to the second stage are the most probable estimates of transmit antenna index and modulated symbol, the high performance inherent to SM-OD is still maintained. Note that the MS detector is proposed specifically for a four transmit multiple receive antenna SM architecture with high order M-QAM, however, MS detection is a generic concept that can be applied to any SM configuration.

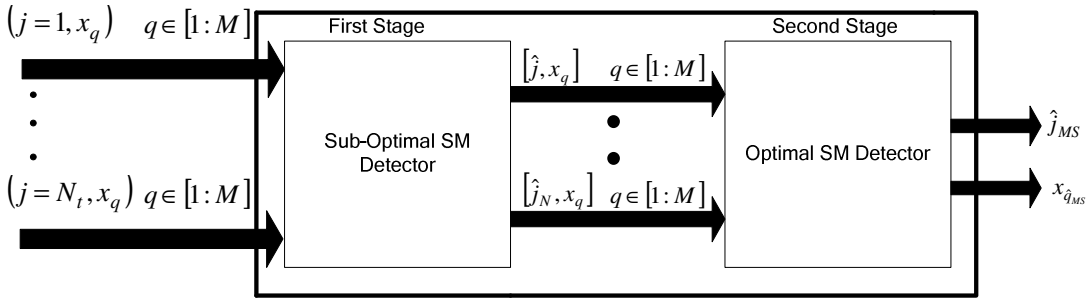

Figure 4-1 Multiple-Stage Detector Operation

4.2 First Stage: Sub-optimal SM Detector

In the first stage of MS, the N most probable estimates of transmit antenna index are determined based on the sub-optimal antenna detection algorithm. The trade-off between complexity and performance when choosing a suitable value for N is discussed in Section 4.5. As shown in Section 2.5.2, the sub-optimal antenna detection rules can be applied to the received signal vector as follows:

$$z_j = \frac{\boldsymbol{h}_j^H \boldsymbol{y}}{\|\boldsymbol{h}_j\|_F} \tag{4-1}$$

where $\boldsymbol{y}$ is the received signal vector, $\boldsymbol{h}_j$ denotes the j^{th} column of channel matrix $\boldsymbol{H}$ and $j \in [1:N_t]$.

Based on (4-1) the vector $\boldsymbol{z}$ can be defined as [12, Eq.(5)]:

$$\boldsymbol{z} = [z_1\ z_2\ \dots\dots z_{N_t}]^T \tag{4-2}$$

Assuming noise free transmission, the active transmit antenna will correspond to the index of the maximum absolute value element in (4-2) [12]. However, the aforementioned condition is not always satisfied in non-ideal conditions, thus leading to incorrect transmit antenna

estimation. Depending on the severity of the noise, the active transmit antenna may correspond to the index of the second or even N_t^{th} largest absolute value element in (4-2)**.** In view of this fact, the first stage of MS selects the N most probable estimates of transmit antenna index as opposed to a single estimate. The N transmit antenna estimates and their associated M-ary constellations are then input to the second stage, which applies the optimal SM detection rule to obtain a final estimate of transmit antenna index and modulated symbol.

The N estimates of transmit antenna index are obtained by evaluating:

$$\hat{\boldsymbol{j}} = \underset{j}{argmax\ N}\ \{|z_j|\} \tag{4-3}$$

where the $\underset{j}{argmax\ N}$ operator selects the N values of j which maximize $|z_j|$ and arranges them in a vector $\hat{\boldsymbol{j}}$.

Hence, vector $\hat{\boldsymbol{j}}$ comprises N estimates of transmit antenna index and can be represented by:

$$\hat{\boldsymbol{j}} = [\hat{j}_1 \dots \dots \ \hat{j}_N] \tag{4-4}$$

where $\hat{j}_1$ corresponds to the most probable transmit antenna index estimate and $\hat{j}_N$ the least probable estimate.

4.3 Second Stage: Optimal SM Detector

The second stage of MS detection utilizes the optimal SM detector to obtain a final estimate of transmit antenna index and modulated symbol as follows [14, Eq.(4)]:

$$\left[\hat{j}_{MS}\ ,\ x_{\hat{q}_{MS}}\right] = \underset{\hat{j}_l\ ,q}{argmin}\ \ \left[\sqrt{p}\left\|\boldsymbol{g}_{\hat{j}_l q}\right\|_F^2 - 2Re\{\boldsymbol{y}^H \boldsymbol{g}_{\hat{j}_l q}\}\right] \tag{4-5}$$

where p is the average SNR at each receive antenna, $\boldsymbol{g}_{\hat{j}_l q} = \boldsymbol{h}_{\hat{j}_l} x_q$ with $l \in [1{:}N]$ and $q \in [1{:}M]$. $\hat{j}_{MS}$ and $x_{\hat{q}_{MS}}$ denote the final estimates of transmit antenna index and symbol, respectively.

4.4 Performance Comparison: SM Detection Schemes

The aim of this section is to validate the claimed advantages of MS detection through Monte Carlo simulation results. The simulations are performed over an i.i.d Rayleigh flat fading channel with AWGN, where the average BER is plotted against the average SNR at each receive antenna. The following were assumed during simulation: the channel matrix $\boldsymbol{H}$ and AWGN vector $\boldsymbol{n}$ comprise i.i.d entries distributed according to $\mathcal{CN}(0,1)$; Gray Coded M-QAM constellation; full channel knowledge at receiver; transmit and receive antennas are separated wide enough to avoid correlation and the total transmit power is the same for all transmissions.

Figure 4-2 shows the BER performance of 4×4 16-QAM SM using the various SM detection schemes discussed in this dissertation. The first notable observation is that the sub-optimal SM detector exhibits reduced performance (approximately 4 dB at a BER of 10^{-5}) as compared to SM-OD. It can also be seen that the $N = 1$ MS detector achieves the same performance as sub-optimal detection. The first stage of N=1 MS detection computes a single transmit antenna index estimate by evaluating (4-1) and (4-3). These are equivalent to the sub-optimal antenna detection rules given by (2-24) and (2-25). In the second stage, the N=1 MS detector computes (4-5) in order to obtain a symbol estimate. It can be shown that (4-5) is equivalent to the sub-optimal detection rule (2-23). Hence, the N = 1 MS detector reduces to sub-optimal SM detection, since both schemes use equivalent rules for detection. The MS detector with N = 2 or 3 achieves virtually the same BER performance as SM-OD. The reason for this behaviour is that the MS detection scheme utilizes an optimal detector in its second stage. This optimal detector operates on a restricted input of most probable transmit antenna and symbol estimates. As a result, the MS detector achieves optimal performance at a reduced complexity.

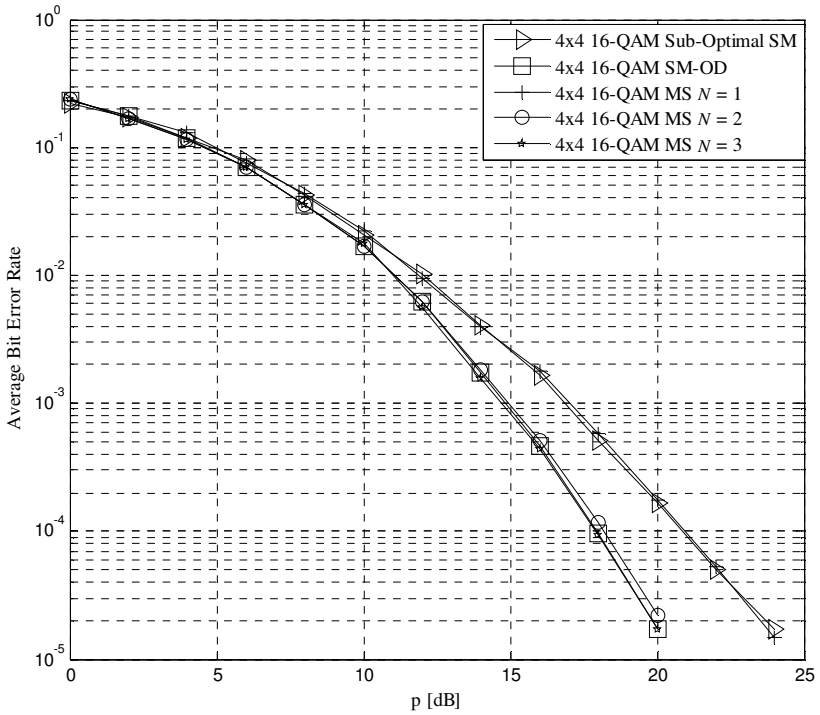

Figure 4-2 BER Performance of 4x4 16-QAM SM Using Various SM Detectors

The average BER performance of 4×4 64-QAM SM using the various SM detection schemes is shown in Figure 4-3. Similar to the results in Figure 4-2, the $N = 1$ MS detector performs as the sub-optimal detector and the $N = 2$ or 3 MS detector performs the same as the SM-OD scheme.

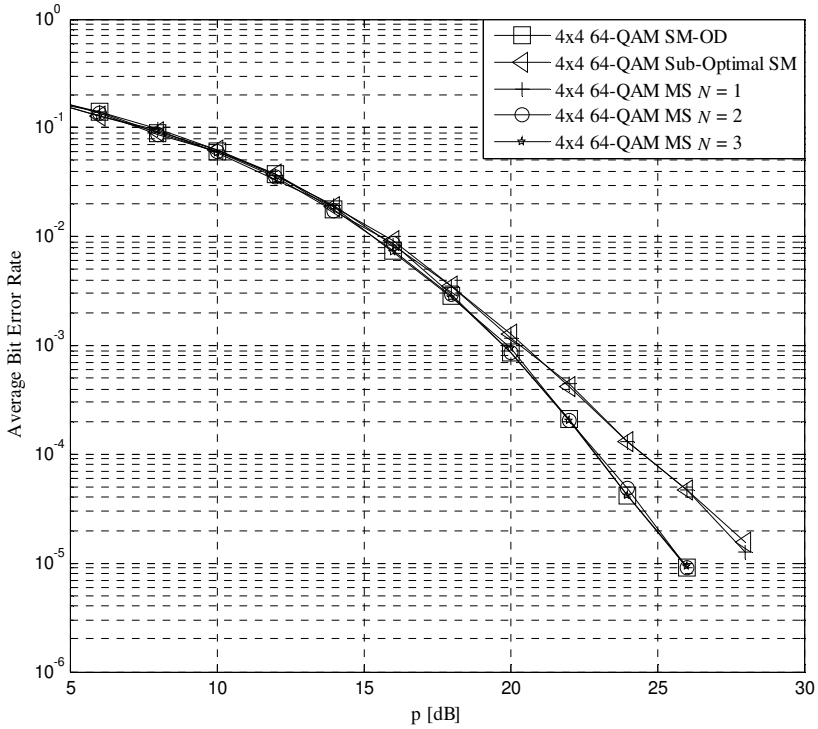

Figure 4-3 BER Performance of 4x4 64-QAM SM Using Various SM detectors

4.5 Complexity Analysis

The complexity of sub-optimal, optimal and multiple-stage detection schemes are compared in this section. The complexity computation is similar to the analysis performed in [12] and [28], where only addition and multiplication of complex numbers are considered as operations.

4.5.1 Sub-Optimal SM Detector

The sub-optimal detection rules are given in Section 2.5.2 as:

$$z_j = \frac{\boldsymbol{h}_j{}^H \boldsymbol{y}}{\|\boldsymbol{h}_j\|_F} \tag{4-6}$$

where $\boldsymbol{y}$ is the received signal vector, $\boldsymbol{h}_j$ denotes the j^{th} column of channel matrix $\boldsymbol{H}$ and $j \in [1: N_t]$.

$$\hat{j} = \underset{j}{argmax} |z_j| \tag{4-7}$$

where $\hat{j}$ represents the estimated transmit antenna index.

$$\tilde{x} = \|\boldsymbol{h}_{\hat{j}}\|_F \, z_{\hat{j}} \tag{4-8}$$

where $\tilde{x}$ denotes the combined symbol based on MRRC.

$$x_{\hat{q}} = \underset{q}{argmin} \quad \sqrt{p}\|\boldsymbol{h}_j x_q\|_F^2 - 2Re\{\tilde{x}\, x_q^*\} \tag{4-9}$$

where $x_{\hat{q}}$ represents the modulated symbol estimate and $q \epsilon [1: M]$.

It was shown in [12] that the numerator of (4-6) requires N_r complex multiplications and $(N_r - 1)$ complex additions. The Frobenius norm in the denominator of (4-6) is obtained by first multiplying a vector of length N_r with its complex conjugate and then taking the square root. This results in N_r complex multiplications and zero complex additions. (4-6) is

evaluated for $j\epsilon[1:N_t]$ and therefore needs a total of $2N_tN_r + N_t(N_r - 1)$ complex operations. The absolute value operation in (4-7) requires one complex multiplication and zero complex additions. (4-7) is also evaluated for $j\epsilon[1:N_t]$ and thus requires N_t complex operations [28]. Summing the complexity contributions of (4-6) and (4-7) yields the total complexity for antenna detection as:

$$\delta_{ant} = 2N_tN_r + N_t(N_r - 1) + N_t = 3N_tN_r \tag{4-10}$$

The complexity of signal combining in (4-8) is negligible since z_j and $\|\boldsymbol{h}_j\|_F$ have been calculated previously in (4-6). Furthermore, the multiplication of z_j by $\|\boldsymbol{h}_j\|_F$ is a non-complex operation that does not contribute to the overall complexity.

The symbol estimate is obtained by evaluating (4-9). As in [14], the first term is simplified by splitting $\|\boldsymbol{h}_j x_q\|_F^2 = \|\boldsymbol{h}_j\|_F^2 |x_q|^2$. The complexity of $\|\boldsymbol{h}_j\|_F^2$ is ignored since $\|\boldsymbol{h}_j\|_F$ has been computed previously in (4-6) and the squaring of $\|\boldsymbol{h}_j\|_F$ is a non-complex operation. The calculation of $|x_q|^2$ involves one complex multiplication and zero complex additions. This operation is performed for $q\epsilon[1:M]$ and therefore needs M complex operations. Note that the complexity of computing $\sqrt{p}\|\boldsymbol{h}_j\|_F^2 |x_q|^2$ is not considered, since it requires the multiplication of non-complex quantities. In the second term of (4-9), $\tilde{x}\, x_q^*$ is evaluated for $q\epsilon[1:M]$ and therefore requires M complex multiplications and zero complex additions. Thus, the complexity of symbol detection can be expressed as:

$$\delta_{symbol} = 2M \tag{4-11}$$

Hence, the total computational complexity of sub-optimal SM detection is given by:

$$\delta_{sub-opt} = \delta_{ant} + \delta_{symbol} = 3N_tN_r + 2M \tag{4-12}$$

4.5.2 Optimal SM Detector

The ML based SM detection rule given in Section 2.5.3 as:

$$[\hat{j}, x_{\hat{q}}] = \underset{j,q}{argmin} \left[\sqrt{p}\left\|\boldsymbol{h}_j x_q\right\|_F^2 - 2Re\{\boldsymbol{y}^H \boldsymbol{h}_j x_q\}\right] \tag{4-13}$$

where $\hat{j}$ and $x_{\hat{q}}$ represent the estimated transmit antenna index and symbol based on ML, respectively, $j \epsilon [1: N_t]$ and $q \epsilon [1: M]$.

As in [14], the first term of (4-13) is simplified by splitting $\left\|\boldsymbol{h}_j x_q\right\|_F^2 = \left\|\boldsymbol{h}_j\right\|_F^2 |x_q|^2$. The squared Frobenius norm operation $\left\|\boldsymbol{h}_j\right\|_F^2$ requires N_r complex multiplications and zero complex additions. $\left\|\boldsymbol{h}_j\right\|_F^2$ is evaluated for $j \epsilon [1: N_t]$ and therefore needs $N_t N_r$ complex multiplications and zero complex additions. The computation of $|x_q|^2$ requires one complex multiplication and zero complex additions. This operation is performed for $q \epsilon [1: M]$ and therefore involves M complex multiplications and zero complex additions. Hence, the first term of (4-13) has complexity [14]:

$$\delta_{opt\_term1} = N_t N_r + M \tag{4-14}$$

The complexity of term two in (4-13) is dependent on the calculation of $\left(\boldsymbol{y}^H \boldsymbol{h}_j\right)\boldsymbol{x}_q$. The $\boldsymbol{y}^H \boldsymbol{h}_j$ operation is performed for $j \epsilon [1: N_t]$ and therefore needs $N_t N_r$ complex multiplications and $N_t(N_r - 1)$ complex additions. It can be shown that the multiplication of $\boldsymbol{y}^H \boldsymbol{h}_j$ by $\boldsymbol{x}_q$ requires $N_t M$ complex multiplications [14] and zero complex additions. Hence, the second term has complexity:

$$\delta_{opt\_term2} = N_t(2N_r + M - 1) \tag{4-15}$$

Therefore, the total computational complexity of SM-OD is given by:

$$\delta_{opt} = \delta_{opt\_term1} + \delta_{opt\_term2} = N_t(3N_r + M - 1) + M \tag{4-16}$$

4.5.3 Multiple-Stage Detector

The first stage of MS detection utilizes the sub-optimal antenna detection algorithm given in Section 4.2 as:

$$z_j = \frac{\boldsymbol{h}_j^H \boldsymbol{y}}{\|\boldsymbol{h}_j\|_F} \tag{4-17}$$

where $\boldsymbol{y}$ is the received signal vector, $\boldsymbol{h}_j$ denotes the j^{th} column of channel matrix $\boldsymbol{H}$ and $j \in [1: N_t]$.

$$\hat{\boldsymbol{j}} = \underset{j}{argmax\ N}\ \{|z_j|\} \tag{4-18}$$

where $\hat{\boldsymbol{j}} = [\hat{j}_1 \ldots \ldots \ \hat{j}_N]$ represents a vector of N transmit antenna index estimates.

As shown in (4-10), the complexity of the first stage given by:

$$\delta_{First\_Stage} = \delta_{ant} = 3N_t N_r \tag{4-19}$$

In the second stage, the MS detector applies the optimal SM detection rule given in Section 4.3 as:

$$[\hat{j}_{MS}\ ,\ x_{\hat{q}_{MS}}] = \underset{\hat{j}_l\ ,q}{argmin}\ \ \left[\sqrt{p}\|\boldsymbol{h}_{\hat{j}_l} x_q\|_F^2 - 2Re\{\boldsymbol{y}^H \boldsymbol{h}_{\hat{j}_l} x_q\}\right] \tag{4-20}$$

where $\hat{j}_{MS}$ and $x_{\hat{q}_{MS}}$ denote the final estimates of transmit antenna index and symbol, respectively, $l\ \epsilon[1: N]$ and $q\epsilon[1: M]$.

Term one of (4-20) is simplified by splitting $\|\boldsymbol{h}_{\hat{j}_l} x_q\|_F^2 = \|\boldsymbol{h}_{\hat{j}_l}\|_F^2 |x_q|^2$ [14]. The calculation of $|x_q|^2$ requires one complex multiplication and zero complex additions. $|x_q|^2$ is evaluated for $q\epsilon[1: M]$ and therefore term one needs M complex operations. Note that the computation of $\|\boldsymbol{h}_{\hat{j}_l}\|_F^2$ is not considered, since $\|\boldsymbol{h}_{\hat{j}_l}\|_F$ has been computed previously in (4-17). Furthermore, the squaring of $\|\boldsymbol{h}_{\hat{j}_l}\|_F$ is a non-complex operation that does not contribute to the overall complexity.

The complexity of term two in (4-20) can be obtained from (4-15) by replacing N_t with N and this yields $N(2N_r + M - 1)$. Therefore, the computational complexity of the second stage is given by:

$$\delta_{Second\_Stage} = N(2N_r + M - 1) + M \tag{4-21}$$

Summing the complexity contributions of the first and second stages yields the total complexity of MS detection as:

$$\delta_{MS} = \delta_{First\_Stage} + \delta_{Second\_Stage} = 3N_tN_r + N(2N_r + M - 1) + M \tag{4-22}$$

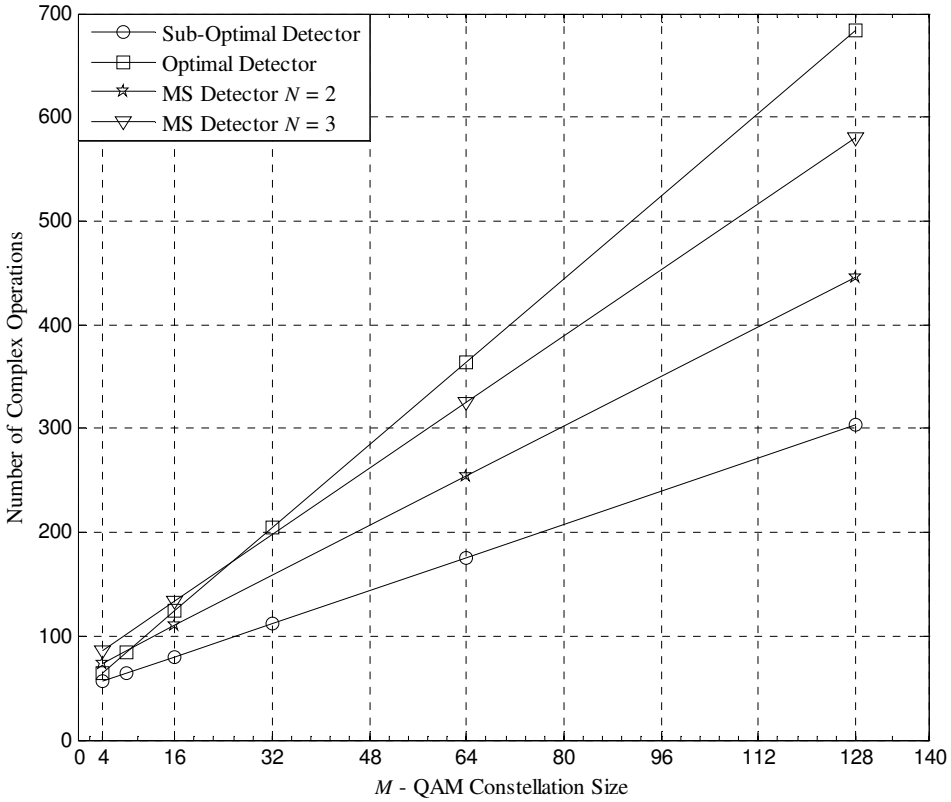

Figure 4-4 Complexity of Sub-optimal, Optimal and Multiple-stage Detection Schemes for the 4×4 M-QAM SM Configuration

Figure 4-4 shows the complexity of various SM detection schemes for fixed 4×4 antenna configuration and variable M-QAM constellation size. It can be seen that optimal, sub-optimal and multiple-stage detection schemes have comparable complexity for low order M-QAM $(M \leq 4)$. However, the optimal detector requires significantly more complex operations for high order M-QAM $(M \geq 16)$. For example, at M = 128 the sub-optimal SM

detection requires 304 complex operations. For the same modulation order, the optimal detector requires 684 complex operations (approximately 125% increase in complexity). Therefore, SM-OD is not practical for high order M-QAM SM systems. In Section 4.4, simulation results demonstrated that both $N = 2$ and $N = 3$ MS detectors achieve similar performance to SM-OD. However, the $N = 2$ MS detector is less complex as compared to $N = 3$ MS and SM-OD. Generally, it can be stated that for any $4 \times N_r$ M-QAM SM system with $M \geq 16$ the $N = 2$ MS detector offers optimal performance at significantly reduced complexity as compared to SM-OD. To quantify our findings numerical complexity results are shown in Table 4-1.

Table 4-1. Complexity of Sub-optimal, Optimal and Multiple-Stage Detectors for the 4×4 M-QAM SM configuration

4x4 SM	16-QAM	64-QAM	128-QAM
Sub-Optimal	80	176	304
Optimal	124	364	684
Multiple-Stage N=2	110	254	446
Multiple-Stage N=3	133	325	581

As compared to SM-OD, the $N = 2$ MS detector reduces complexity by approximately 11%, 30% and 35% for the 16, 64 and 128-QAM constellations, respectively. On the other hand, sub-optimal detection has a lower complexity than $N = 2$ MS detection but this is offset by reduced performance, as shown in Section 4.4.

4.6 Chapter Summary

A multiple-stage detection scheme for high order M-QAM SM configurations ($M \geq 16$) was proposed in this chapter. Complexity analyses and Monte Carlo simulations have shown that the MS detector with $N = 2$ is optimal for the $4 \times N_r$ SM configuration, since it attains the same BER performance and up to a 35% reduction in receiver complexity as compared to

SM-OD. The next chapter presents a novel SM based technique, which outperforms the conventional SM-OD scheme in terms of BER.

Chapter 5

Alamouti Coded Spatial Modulation

Conventional SM schemes transmit data via a single antenna and therefore do not fully exploit the transmit diversity provided by the MIMO channel. This motivates the development for a performance enhanced SM technique, which obtains transmit diversity by simultaneously transmitting data from multiple antennas. The proposed scheme termed ACSM implements the Alamouti STBC [6] transmit diversity technique in conjunction with SM. Thus, ACSM obtains both transmit and receive diversity as compared to conventional SM where only receive diversity is achieved.

This chapter is outlined as follows: Section 5.1 describes the ACSM system model and provides a detailed explanation of the transmission and detection processes. The complexity of ACSM, Alamouti STBC and SM-OD is then analyzed in Section 5.2. Section 5.3 presents an asymptotic performance bound for real constellation ACSM schemes and the accuracy of this bound is investigated in Section 5.4. Section 5.5 shows a performance comparison between the various transmission schemes and finally, a chapter summary is given in Section 5.6.

5.1 System Model

ACSM is a novel MIMO transmission technique based on the principle of SM. Unlike conventional SM techniques, ACSM offers transmit diversity by utilizing Alamouti STBC in conjunction with SM. The basic idea behind ACSM is to map a block of information bits to a set of two transmit antennas (spatial domain) and a pair of modulated symbols (signal domain). The mapping process is defined by an SM mapping table, which is assumed to be known at both transmitter and receiver. The modulated symbols are then encoded and transmitted by the specified transmit antenna set as per the Alamouti STBC scheme. Alamouti STBC is orthogonal by design, hence ACSM schemes efficiently avoid the effects of ICI. However, the use of Alamouti STBC requires IAS, which increases overhead at the transmitter. At the receiver end, the ACSM detector estimates the active transmit antenna set index and the transmitted symbols, thereby allowing for the recovery of the original information bits. The proposed technique can be used in conjunction with most digital

modulation schemes, for example *M*-QAM and *M*-PSK, however analysis will be restricted to real constellation (BPSK) ACSM configurations.

5.1.1 Transmission

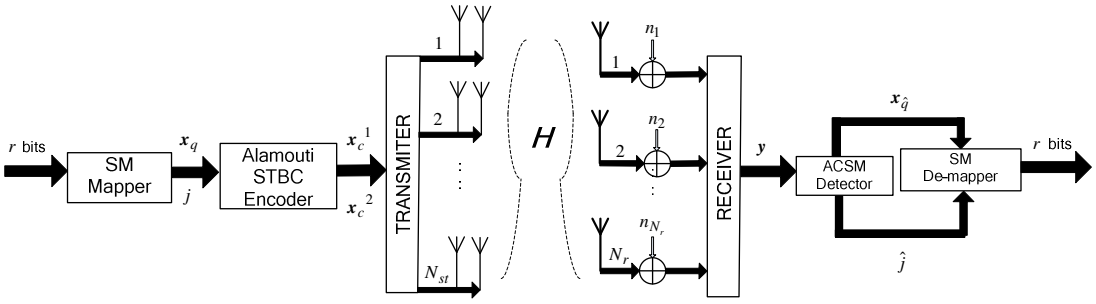

Figure 5-1 ACSM System Model

Figure 5-1 shows the system model for an $N_{st} \times N_r$ ACSM scheme. Herein, the $N_{st} \times N_r$ configuration refers to an ACSM system comprising N_{st} transmit antenna sets (note that each set has two transmit antennas) and N_r receive antennas, respectively. Initially, the SM mapper uses an SM mapping table (refer to Section 5.1.3) to assign a block of r information bits to a transmit antenna set index j and a two dimensional symbol vector $\boldsymbol{x}_q$.

$$\boldsymbol{x}_q = \left[x_{q1}\ x_{q2}\right]^T \tag{5-1}$$

where $\boldsymbol{x}_q$ refers to the q^{th} combination of modulated symbols x_{q1} and x_{q2}, which stem from an M-ary constellation and $q \epsilon [1: M^2]$.

In general, the number of bits that can be transmitted using ACSM is given by:

$$r = log_2\ (M^2 N_{st}) \tag{5-2}$$

As in conventional SM, the number of transmit antenna sets or digital modulation scheme can be adjusted to achieve a desired transmission rate. For example 4×4 16-QAM ACSM transmits 10 databits in two time slots, which results in a transmission rate of 5 bps. Alternatively, if channel conditions do not permit the use of 16-QAM, the same transmission rate can be achieved by the 16×4 8-QAM ACSM configuration.

The SM mapper output can be represented by a $2N_{st}$ dimensional signal vector as follows:

$$\boldsymbol{x}_{jq} = \begin{bmatrix} 0 & 0 & \dots & x_{q1} & x_{q2} & \dots & 0 & 0 \end{bmatrix}^T \quad (5\text{-}3)$$

(j^{th} position ↓ above x_{q1}; ↑ 1^{st} position; ↑ $N_{st}{}^{th}$ position)

where j represents the mapped transmit antenna set index. Note that a particular position will refer to a pair of elements in $\boldsymbol{x}_{jq}$. In general, the 1^{st} position refers to the first 2 elements in $\boldsymbol{x}_{jq}$ and the j^{th} position will refer to the j^{th} pair of elements in $\boldsymbol{x}_{jq}$.

The SM mapper output is then passed to the Alamouti STBC encoder, which encodes the symbol vector $\boldsymbol{x}_q$ as follows:

$$\boldsymbol{x}_c^1 = \begin{bmatrix} x_{q1} & x_{q2} \end{bmatrix}^T \quad (5\text{-}4)$$

where $\boldsymbol{x}_c^1$ denotes the encoded symbol vector in the first time slot.

$$\boldsymbol{x}_c^2 = \begin{bmatrix} -x_{q2}^* & x_{q1}^* \end{bmatrix}^T \quad (5\text{-}5)$$

where $\boldsymbol{x}_c^2$ denotes the encoded symbol vector in the second time slot.

The ACSM scheme requires two time slots for the transmission of two symbols. In the first time slot, $\boldsymbol{x}_c^1 = \begin{bmatrix} x_{q1} & x_{q2} \end{bmatrix}^T$ is simultaneously transmitted over the MIMO channel by the first and second antennas from transmit antenna set j, respectively. During the second time slot $\boldsymbol{x}_c^2 = \begin{bmatrix} -x_{q2}^* & x_{q1}^* \end{bmatrix}^T$ is then transmitted via the first and second antennas from transmit antenna set j, respectively. Note that only one transmit antenna set is active during an ACSM transmission. Therefore, at any instant the $N_{st} \times N_r$ ACSM configuration may be viewed as a $2 \times N_r$ MIMO architecture.

The MIMO channel is modelled by an $N_r \times 2N_{st}$ dimensional fading coefficient matrix $\boldsymbol{H}$. The channel matrix $\boldsymbol{H}$ is composed of N_{st} sub-matrices $\boldsymbol{h}_j$, where each $N_r \times 2$ dimensional sub-matrix $\boldsymbol{h}_j$ corresponds to the channel path gains between the first and second transmit antennas from set j and their corresponding receive antennas.

$$\boldsymbol{H} = \left[\boldsymbol{h}_1 \dots \boldsymbol{h}_j \dots \boldsymbol{h}_{N_{st}}\right] \tag{5-6}$$

where $\boldsymbol{h}_j = \begin{bmatrix} h_{1,j1}\, h_{2,j1} \dots \dots h_{N_r,j1} \\ h_{1,j2}\, h_{2,j2} \dots \dots h_{N_r,j2} \end{bmatrix}^T$ and indices $j1$ and $j2$ denote the first and second transmit antennas from the j^{th} transmit antenna set, respectively.

Assuming transmission from the j^{th} transmit antenna set and constant fading coefficients over two consecutive time slots, the received signal vectors in the first and second time slots are as follows:

First time slot:

$$\boldsymbol{y}^1 = \sqrt{p}\boldsymbol{h}_j \boldsymbol{x}_c^1 + \boldsymbol{n}^1 \tag{5-7}$$

where $\boldsymbol{y}^1 = \left[y_1^1\, y_2^1 \dots y_{N_r}^1\right]^T$ is the received signal vector in the first time slot, p is the average SNR at each receive antenna , $\boldsymbol{n}^1 = \left[n_1^1\, n_2^1 \dots n_{N_r}^1\right]^T$ denotes the N_r dimensional AWGN vector and $E[|\boldsymbol{x}_c^1|^2] = 1$ to ensure unity transmit power.

Second time slot:

$$\boldsymbol{y}^2 = \sqrt{p}\boldsymbol{h}_j \boldsymbol{x}_c^2 + \boldsymbol{n}^2 \tag{5-8}$$

where $\boldsymbol{y}^2 = \left[y_1^2\, y_2^2 \dots y_{N_r}^2\right]^T$ is the received signal vector in the second time slot, $\boldsymbol{n}^2 = \left[n_1^2\, n_2^2 \dots n_{N_r}^2\right]^T$ denotes the N_r dimensional AWGN vector and $E[|\boldsymbol{x}_c^2|^2] = 1$ to ensure unity transmit power. Note that $\boldsymbol{H}$, $\boldsymbol{n}^1$ and $\boldsymbol{n}^2$ have i.i.d entries according to $\mathcal{CN}(0,1)$.

For notational convenience the received signal vectors in the first and second time slots can also be represented by:

$$\begin{bmatrix} y_1^1 \\ y_2^1 \\ \vdots \\ y_{N_r}^1 \\ y_1^{*2} \\ y_2^{*2} \\ \vdots \\ y_{N_r}^{*2} \end{bmatrix} = \sqrt{p} \begin{bmatrix} h_{1,j1} & h_{1,j2} \\ h_{2,j1} & h_{2,j2} \\ \vdots & \vdots \\ h_{N_r,j1} & h_{N_r,j2} \\ h_{1,j2}^* & -h_{1,j1}^* \\ h_{2,j2}^* & -h_{2,j1}^* \\ \vdots & \vdots \\ h_{N_r,j2}^* & -h_{N_r,j1}^* \end{bmatrix} \begin{bmatrix} x_{q1} \\ x_{q2} \end{bmatrix} + \begin{bmatrix} n_1^1 \\ n_2^1 \\ \vdots \\ n_{N_r}^1 \\ n_1^{*2} \\ n_2^{*2} \\ \vdots \\ n_{N_r}^{*2} \end{bmatrix} \tag{5-9}$$

Rewriting (5-9) in matrix notation yields:

$$\boldsymbol{y} = \sqrt{p}\boldsymbol{h}_{c_j}\boldsymbol{x}_q + \boldsymbol{n} \tag{5-10}$$

where $\boldsymbol{y}$ is a $2N_r$ dimensional vector, which represents the received signals in the first and second time slots, respectively, $\boldsymbol{n}$ denotes the $2N_r$ dimensional AWGN vector and $\boldsymbol{h}_{c_j} = \begin{bmatrix} h_{1,j1} & h_{2,j1} \dots h_{N_r,j1} & h_{1,j2}^* & h_{2,j2}^* & \dots & h_{N_r,j2}^* \\ h_{1,j2} & h_{2,j2} \dots & h_{N_r,j2} & -h_{1,j1}^* & -h_{2,j1}^* \dots & -h_{N_r,j1}^* \end{bmatrix}^T$.

Similar to $\boldsymbol{H}$, we can define the $2N_r \times 2N_{st}$ dimensional matrix $\boldsymbol{H}_c$ as:

$$\boldsymbol{H}_c = \left[\boldsymbol{h}_{c_1}\, \boldsymbol{h}_2 \dots \boldsymbol{h}_{c_j} \dots \boldsymbol{h}_{c_{N_{st}}}\right] \tag{5-11}$$

Rewriting (5-10) in terms of (5-11) and (5-3) yields:

$$\boldsymbol{y} = \sqrt{p}\boldsymbol{H}_c\boldsymbol{x}_{jq} + \boldsymbol{n} \tag{5-12}$$

5.1.2 Detection

The ACSM detector implements the following ML based rule for the estimation of transmit antenna set index and symbol vector:

$$\left[\hat{j}\,, \boldsymbol{x}_{\hat{q}}\right] = \underset{}{argmax}\; p_Y\left(\boldsymbol{y}\middle|\boldsymbol{x}_{jq}, \boldsymbol{H}_c\right)$$

$$= \underset{j,q}{argmin} \left[\sqrt{p}\left\|\boldsymbol{g}_{jq}\right\|_F^2 - 2Re\left\{\boldsymbol{y}^H\boldsymbol{g}_{jq}\right\}\right] \tag{5-13}$$

where $\hat{j}$ and $\boldsymbol{x}_{\hat{q}}$ represent the estimated transmit antenna set index and symbol vector based on ML, respectively, $\boldsymbol{g}_{jq=}\boldsymbol{h}_{c_j}\boldsymbol{x}_q$, $j \in [1: N_{st}]$, $q \in [1: M^2]$ and $p_Y(\boldsymbol{y}|\boldsymbol{x}_{jq}, \boldsymbol{H}_c) = \pi^{-Nr} exp\left(-\|\boldsymbol{y} - \sqrt{p}\boldsymbol{H}_c\boldsymbol{x}_{jq}\|_F^2\right)$ is the PDF of the received signal vector $\boldsymbol{y}$ conditioned on both $\boldsymbol{x}_{jq}$ and $\boldsymbol{H}_c$.

The estimates $\hat{j}$ and $\boldsymbol{x}_{\hat{q}}$ are then passed to the SM de-mapper, which uses the SM mapping table to recover an estimate of the original r bit input.

5.1.3 2×2 BPSK ACSM Transmission and Detection

The SM mapping table for 2×2 BPSK ACSM is shown in Table 5-1. The first column in Table 5-1 contains all variants of the three bit binary input. The second and third columns contain all possible combinations of transmit antenna set index j and symbol vector $\boldsymbol{x}_q$. In ACSM, data is simultaneously transmitted from two antennas, whereas SM uses a single antenna for data transmission. As a result, the total transmit power in ACSM is twice that of SM. In order to draw a fair comparison between the two systems, it is necessary to halve the energy allocated to each ACSM symbol. This is equivalent to scaling the transmitted symbol vector $\boldsymbol{x}_q$ by a factor of $\sqrt{2}$, as shown in column three of Table 5-1.

Table 5-1 SM Mapping Table – 2×2 BPSK ACSM Transmission

Input Bits	j	$\boldsymbol{x}_q$	q
000	1	$[-0.7071 \quad -0.7071]^T$	1
001	1	$[-0.7071 \quad 0.7071]^T$	2
010	1	$[0.7071 \quad -0.7071]^T$	3
011	1	$[0.7071 \quad 0.7071]^T$	4
100	2	$[-0.7071 \quad -0.7071]^T$	1
101	2	$[-0.7071 \quad 0.7071]^T$	2
110	2	$[0.7071 \quad -0.7071]^T$	3
111	2	$[0.7071 \quad 0.7071]^T$	4

In Table 5-1, each binary input sequence is uniquely identified by a combination of transmit antenna set index j and symbol vector $\boldsymbol{x}_q$. Consider the following binary transmission sequence $[0\ 1\ 0]$. The binary sequence is mapped to the first transmit antenna set $(j = 1)$ and symbol vector $\boldsymbol{x}_3 = [\,0.7071 \ -0.7071]^T$. This results in signal vector $\boldsymbol{x}_{jq} = [0.7071 \ \ -0.7071 \ \ 0 \ \ \ 0]^T$. The symbol vector $\boldsymbol{x}_3$ is input to the Alamouti STBC encoder which outputs $\boldsymbol{x}_c^1 = [0.7071 \ -0.7071\,]^T$ and $\boldsymbol{x}_c^2 = [0.7071 \ \ 0.7071\,]^T$ in the first and second time slots, respectively. In the first time slot, $\boldsymbol{x}_c^1$ is simultaneously transmitted over the MIMO channel by the first and second antennas from transmit antenna set one. During the second time slot $\boldsymbol{x}_c^2$ is then transmitted via the first and second antennas from transmit antenna set one. Note that only transmit antenna set one is active during transmission and transmit antenna set two radiates zero energy. Consider ACSM transmission over the following MIMO channel:

$$\boldsymbol{H} = \begin{pmatrix} -0.3059 + 0.2314\text{i} & -0.8107 - 0.4160\text{i} & 0.7543 - 0.4892\text{i} & 0.2082 - 1.0189\text{i} \\ -1.1777 + 0.1235\text{i} & 0.8421 + 1.5437\text{i} & 0.0419 + 0.6067\text{i} & -0.9448 + 0.4039\text{i} \end{pmatrix} \quad (5\text{-}14)$$

Using the relation in (5-11), $\boldsymbol{H}_c$ can be defined as:

$$\boldsymbol{H}_c = \begin{pmatrix} -0.3059 + 0.2314\text{i} & -0.8107 - 0.4160\text{i} & 0.7543 - 0.4892\text{i} & 0.2082 - 1.0189\text{i} \\ -1.1777 + 0.1235\text{i} & 0.8421 + 1.5437\text{i} & 0.0419 + 0.6067\text{i} & -0.9448 + 0.4039 \\ -0.8107 + 0.4160 & 0.3059 + 0.2314\text{i} & 0.2082 + 1.0189\text{i} & -0.7543 - 0.4892\text{i} \\ 0.8421 - 1.5437\text{i} & 1.1777 + 0.1235\text{i} & -0.9448 - 0.4039\text{i} & -0.0419 + 0.6067\text{i} \end{pmatrix} \quad (5\text{-}15)$$

Consider the following scenario: noise free transmission, constant fading coefficients over two consecutive time slots and $p = 1$. The received signal vector is then given by:

$$\boldsymbol{y} = [0.3569 + 0.4578i \;\; -1.4282 - 1.0042i \;\; -0.7895 + 0.1305\text{i} \;\; -0.2373 - 1.1789i]^T \quad (5\text{-}16)$$

At the receiving end, the ACSM detector applies the ML detection rule (5-13) in order to estimate the active transmit antenna set index and transmitted symbol vector as follows:

Table 5-2. Computation of ML Decision Metrics – 2×2 BPSK ACSM

j	$\boldsymbol{x}_q$	$\left[\sqrt{p}\|\boldsymbol{g}_{jq}\|_F^2 - 2Re\{\boldsymbol{y}^H\boldsymbol{g}_{jq}\}\right]$
1	$[-0.7071 \;\; -0.7071]^T$	5.4717
1	$[-0.7071 \;\; 0.7071]^T$	16.4150
1	$[0.7071 \;\; -0.7071]^T$	-5.4717
1	$[0.7071 \;\; 0.7071]^T$	5.4717
2	$[-0.7071 \;\; -0.7071]^T$	3.9139
2	$[-0.7071 \;\; 0.7071]^T$	2.8446
2	$[0.7071 \;\; -0.7071]^T$	3.7861
2	$[0.7071 \;\; 0.7071]^T$	2.7168

The first two columns in Table 5-2 contain all possible combinations of transmit antenna set index and symbol vector. The third column is obtained by computing (5-13), based on the inputs j and $\boldsymbol{x}_q$. The transmit antenna set index and symbol vector are estimated by the combination of j and $\boldsymbol{x}_q$ which yields a minimum value in column three. As shown, the minimum value is -5.4717 and this corresponds to $\hat{\jmath} = 1$ and $\boldsymbol{x}_{\hat{q}} = [0.7071 \;\; -0.7071\,]^T$. Finally, these estimates are passed to the SM-demapper, which uses Table 5-1 to recover the original binary input [0 1 0].

5.2 Complexity Analysis

The receiver complexity of Alamouti STBC, SM-OD and ACSM schemes are compared in this section. The complexity computation is similar to the analysis performed in [12] and [28], where only addition and multiplication of complex numbers are considered as operations. It should be noted that the following complexity analysis is specific to real constellation SM-OD and ACSM schemes.

5.2.1 Alamouti Space-Time Block Code

The Alamouti STBC detection process consists of signal combining followed by ML detection, as shown in Section 2.4.2.

Signal Combining:

$$\tilde{x}_1 = \sum_{k=1}^{N_r} h_{k,1}^{*}\, y_k^1 + h_{k,2}\, y_k^{2^*} \tag{5-17}$$

$$\tilde{x}_2 = \sum_{k=1}^{N_r} h_{k,2}^{*}\, y_k^1 - h_{k,1}\, y_k^{2^*} \tag{5-18}$$

where $\tilde{x}_1$ and $\tilde{x}_2$ denote the combined signals.

ML Detection:

$$x_{\hat{q}_1} = \underset{q_1}{argmin}\, \sqrt{p}\left\|\boldsymbol{H}x_{q_1}\right\|_F^2 - 2Re\{\tilde{x}_1 x_{q_1}^{*}\} \tag{5-20}$$

$$x_{\hat{q}_2} = \underset{q_2}{argmin}\ \sqrt{p}\left\|\boldsymbol{H}x_{q_2}\right\|_F^2 - 2Re\{\tilde{x}_2 x_{q_2}^*\} \tag{5-21}$$

where $x_{\hat{q}_1}$ and $x_{\hat{q}_2}$ represent the estimated symbols with $q_1 \epsilon [1:M]$ and $q_2 \epsilon [1:M]$.

The complexity of signal combining in (5-17) and (5-18) is obtained from [28] as:

$$\delta_{Com} = N_r^2 + 4N_r - 2 \tag{5-22}$$

The ML detection of symbol x_{q_1} is given by (5-20). As in [14], term one is simplified by splitting $\left\|\boldsymbol{H}x_{q_1}\right\|_F^2 = \|\boldsymbol{H}\|_F^2 \left|x_{q_1}\right|^2$. The Frobenius norm $\|\boldsymbol{H}\|_F^2$ is obtained by summing the squares of each element in $\boldsymbol{H}$. This results in $2N_r$ complex multiplications and zero complex additions. The computation of $\left|x_q\right|^2$ requires 1 complex multiplication and zero complex additions. $\left|x_q\right|^2$ is evaluated for $q\epsilon[1:M]$ and therefore needs M complex operations. Hence, the first term of (5-20) involves $2N_r + M$ complex operations. Note that the complexity of computing $\sqrt{p}\|\boldsymbol{H}\|_F^2 \left|x_{q_1}\right|^2$ is not considered, since it requires the multiplication of non-complex quantities. In term two of (5-20), $\tilde{x}_1$ is multiplied by x_{q1}^*. This operation is performed for $q_1 \epsilon[1:M]$ and therefore needs M complex multiplications and zero complex additions.

The ML detection of symbol x_{q2} is given by (5-21). The first term of (5-21) has been calculated previously in (5-20) and is therefore neglected. Similar to (5-20), the second term of (5-21) has M complex multiplications and zero complex additions. complex Therefore, the total complexity of ML detection is given by:

$$\delta_{ML} = 2N_r + 3M \tag{5-23}$$

Summing (5-22) and (5-23) yields the total number of complex operations required for the detection of two symbols as:

$$\delta_{Alamouti} = \delta_{Com} + \delta_{ML} = N_r^2 + 6N_r + 3M - 2 \tag{5-24}$$

5.2.2 Real Constellation Spatial Modulation

As shown in Section 2.5.3, the ML based SM detection rule is given by:

$$[\hat{j}, x_{\hat{q}}] = \underset{j,q}{argmin} \left[\sqrt{p}\left\|\boldsymbol{h}_j x_q\right\|_F^2 - 2Re\{\boldsymbol{y}^H \boldsymbol{h}_j x_q\}\right] \tag{5-25}$$

where $\hat{j}$ and $x_{\hat{q}}$ represent the estimated antenna index and symbol based on ML, respectively, $j \in [1: N_t]$ and $q \in [1: M]$.

The first term is simplified by splitting $\left\|\boldsymbol{h}_j x_q\right\|_F^2 = \left\|\boldsymbol{h}_j\right\|_F^2 \left|x_q\right|^2$ [14]. The Frobenius norm operation $\left\|\boldsymbol{h}_j\right\|_F^2$ requires N_r complex multiplications and zero complex additions. Term one is evaluated for $j \in [1: N_t]$ and therefore requires $N_t N_r$ complex operations. Note that the calculation of $\left|x_q\right|^2$ is ignored since it is a non-complex operation.

The complexity of term two in (5-25) is dependent on the evaluation of $\left(\boldsymbol{y}^H \boldsymbol{h}_j\right) x_q$. The $\boldsymbol{y}^H \boldsymbol{h}_j$ operation is performed for $j \in [1: N_t]$ and therefore needs $N_t N_r$ complex multiplications and $N_t(N_r - 1)$ complex additions. The multiplication of $\boldsymbol{y}^H \boldsymbol{h}_j$ by x_q is a non-complex operation that does not contribute to the complexity of term two. It follows that term two requires $N_t(2N_r - 1)$ complex operations. Therefore, the total computational complexity of real constellation SM-OD is given by:

$$\delta_{SM-OD} = N_t N_r + N_t(2N_r - 1) = N_t(3N_r - 1) \tag{5-26}$$

5.2.3 Real Constellation Alamouti Coded Spatial Modulation

The ML based ACSM detector is given in Section 5.1.2 as:

$$[\hat{j}, \boldsymbol{x}_{\hat{q}}] = \underset{j,q}{argmin} \left[\sqrt{p}\left\|\boldsymbol{h}_{c_j} \boldsymbol{x}_q\right\|_F^2 - 2Re\left\{\boldsymbol{y}^H \boldsymbol{h}_{c_j} \boldsymbol{x}_q\right\}\right] \tag{5-27}$$

where $\hat{j}$ and $\boldsymbol{x}_{\hat{q}}$ represent the estimated transmit antenna set index and symbol vector based on ML, respectively, $j \in [1: N_{st}]$ and $q \in [1: M^2]$.

The $\boldsymbol{h}_{c_j}\boldsymbol{x}_q$ operation in term one involves $2N_r$ complex additions and zero complex multiplications. The Frobenius norm $\left\|\boldsymbol{h}_{c_j}\boldsymbol{x}_q\right\|_F^2$ is then obtained by summing the squares of each element in $\boldsymbol{h}_{c_j}\boldsymbol{x}_q$. This requires $2N_r$ complex multiplications and zero complex additions. Term one is evaluated for each combination of transmit antenna set ($j\epsilon[1:N_{st}]$) and symbol vector ($q\epsilon[1:M^2]$) and therefore requires $4N_{st}N_rM^2$ complex operations.

Term two in (5-27) is computed by $\left(\boldsymbol{y}^H\boldsymbol{h}_{c_j}\right)\boldsymbol{x}_q$. The $\boldsymbol{y}^H\boldsymbol{h}_{c_j}$ operation needs $4N_r$ complex multiplications and $4N_r-2$ complex additions. Here, $\boldsymbol{y}^H\boldsymbol{h}_{c_j}$ is evaluated for $j\epsilon[1:N_{st}]$ and thus requires $N_{st}(8N_r-2)$ complex operations. Finally, the multiplication of $\boldsymbol{y}^H\boldsymbol{h}_{c_j}$ by $\boldsymbol{x}_q$ needs one complex addition and zero complex multiplications. This operation is performed $N_{st}M^2$ times and therefore involves $N_{st}M^2$ complex operations. Hence, term two requires $N_{st}(8N_r-2)+N_{st}M^2$ complex operations. Summing the complexity contributions of the first and second terms of (5-13) yields the total complexity required for the detection of two symbols as:

$$\delta_{ACSM}=4N_{st}N_rM^2+N_{st}(8N_r-2)+N_{st}M^2 \tag{5-28}$$

A complexity comparison between SM-OD, Alamouti STBC and ACSM is shown in Table 5-3. In order to make fair comparisons, each system has a transmission rate of 2 bps and the same number of receive antennas. The 2x4 4-QAM Alamouti STBC scheme transmits 4 data bits over two time slots and this requires 50 complex operations for detection. It follows that the detection of 2 bits in one time slot requires 25 complex operations. Similarly, 4x4 BPSK ACSM transmits 4 data bits over two time slots and this requires 392 complex operations for detection. Therefore, the detection of 2 bits needs 196 complex operations.

Table 5-3: Complexity Comparison for 2 bps Transmission

	2x4 BPSK SM-OD	2x4 4QAM Alamouti STBC	4x4 BPSK ACSM
δ	22	25	196

It can be seen that ACSM has a much higher complexity as compared to SM-OD and Alamouti STBC. However, the drawback of high computational complexity is offset by the significant performance gains achievable by ACSM, as shown in Section 5.5.

5.3 Asymptotic Performance Analysis

In this section, an analytical upper bound for the average BER of ACSM over i.i.d Rayleigh flat fading channels is presented. The subsequent analysis is based on the well known union bounding technique and follows a similar approach to the derivation performed in [14]. The average BER of ACSM is union bounded by [32, pp. 261-262]:

$$P_{e,bit} \leq E_x\left[\sum_{\hat{j}\hat{q}} N(\boldsymbol{x}_q, \boldsymbol{x}_{\hat{q}})\, P(\boldsymbol{x}_{jq} \rightarrow \boldsymbol{x}_{\hat{j}\hat{q}})\right]$$

$$= \sum_{j=1}^{N_{st}} \sum_{q=1}^{M^2} \sum_{\hat{j}=1}^{N_{st}} \sum_{\hat{q}=1}^{M^2} \frac{N(\boldsymbol{x}_q, \boldsymbol{x}_{\hat{q}})\, P(\boldsymbol{x}_{jq} \rightarrow \boldsymbol{x}_{\hat{j}\hat{q}})}{N_{st} M^2} \tag{5-29}$$

where $P(\boldsymbol{x}_{jq} \rightarrow \boldsymbol{x}_{\hat{j}\hat{q}})$ denotes the PEP of choosing signal vector $\boldsymbol{x}_{\hat{j}\hat{q}}$ given that $\boldsymbol{x}_{jq}$ was transmitted and $N(\boldsymbol{x}_q, \boldsymbol{x}_{\hat{q}})$ is the number of bits in error between symbol vector $\boldsymbol{x}_q$ and estimated symbol vector $\boldsymbol{x}_{\hat{q}}$.

The PEP conditioned on channel matrix $\boldsymbol{H}$ can be expressed as [14]:

$$P(\boldsymbol{x}_{jq} \rightarrow \boldsymbol{x}_{\hat{j}q} | \boldsymbol{H}_c) = Q(\sqrt{k}) \tag{5-30}$$

where $Q(x) = \int_x^\infty \frac{1}{\sqrt{2\pi}} e^{-t^2/2}\, dt$ and $k = \frac{p}{2} \left\| \boldsymbol{h}_{c_j} \boldsymbol{x}_q - \boldsymbol{h}_{c_{\hat{j}}} \boldsymbol{x}_{\hat{q}} \right\|_F^2 = \frac{p}{2} \left\| \boldsymbol{g}_{jq} - \boldsymbol{g}_{\hat{j}\hat{q}} \right\|_F^2$

The random variable k can be written in terms of its real and imaginary components as follows:

$$k = \sum_{n=1}^{2N_r} |A(n) + iB(n)|^2 \tag{5-31}$$

where

$$A(n) = \sqrt{\frac{p}{2}}\left(h^R_{c_{n,j1}} x^R_{q_1} + h^R_{c_{n,j2}} x^R_{q_2} - h^R_{c_{n,\hat{j}1}} x^R_{\hat{q}_1} - h^R_{c_{n,\hat{j}2}} x^R_{\hat{q}_2}\right) \tag{5-32}$$

$$B(n) = \sqrt{\frac{p}{2}}\left(h^I_{c_{n,j1}} x^R_{q_1} + h^I_{c_{n,j2}} x^R_{q_2} - h^I_{c_{n,\hat{j}1}} x^R_{\hat{q}_1} - h^I_{c_{n,\hat{j}2}} x^R_{\hat{q}_2}\right) \tag{5-33}$$

The superscripts R and I represent the real and imaginary components, respectively. The channel gains $h_{c_{n,j1}}$ and $h_{c_{n,j2}}$ correspond to the elements of $\boldsymbol{h}_{c_j}$ in the n^{th} row and 1^{st} and 2^{nd} columns, respectively.

Since $A(n)$ and $B(n)$ are independent, k reduces to:

$$k = \sum_{n=1}^{4N_r} \alpha_n^2 \tag{5-34}$$

where $\alpha_n \sim N\,(0, \sigma_\alpha^2)$ with $\sigma_\alpha^2 = \frac{p\left(\left|x^R_{q_1}\right|^2 + \left|x^R_{\hat{q}_1}\right|^2 + \left|x^R_{q_2}\right|^2 + \left|x^R_{\hat{q}_2}\right|^2\right)}{4}$.

The random variable k is the summation of $4N_r$ squared i.i.d Gaussian random variables. Hence, k has a central Chi-square distribution with $4N_r$ degrees of freedom and PDF given by [32, p. 41]:

$$p_k(v) = \frac{v^{2N_r - 1} e^{-v/2\sigma_\alpha^2}}{(2\sigma_\alpha^2)^{2N_r}\Gamma(2N_r)} \quad for\ \ v > 0 \tag{5-35}$$

where $\Gamma(2N_r) = \int_0^\infty t^{2N_r - 1} e^{-t} dt$ is the gamma function.

Since k has a known distribution, the PEP term in (5-29) can be computed by averaging the conditional PEP $P\left(\boldsymbol{x}_{jq} \to \boldsymbol{x}_{\hat{j}\hat{q}} \middle| \boldsymbol{H}_c\right)$ over the PDF of k [14].

$$P\left(\boldsymbol{x}_{jq} \to \boldsymbol{x}_{\hat{j}\hat{q}}\right) = \int_{v=0}^{\infty} Q\left(\sqrt{v}\right) p_k(v) dv \tag{5-36}$$

where $Q(x) = \int_x^\infty \frac{1}{\sqrt{2\pi}} e^{-t^2/2}\, dt$

The closed form solution for (5-36) is given in [33, Eq. (64)]:

$$P\left(\boldsymbol{x}_{jq} \rightarrow \boldsymbol{x}_{\hat{j}\hat{q}}\right) = \mu_{\alpha}^{2N_r} \sum_{w=0}^{2N_r-1} \binom{2N_r - 1 + w}{w} [1-\mu_{\alpha}]^{w} \tag{5-37}$$

where $\mu_{\alpha} = \frac{1}{2}\left(1 - \sqrt{\frac{\sigma_{\alpha}^2}{1+\sigma_{\alpha}^2}}\right)$.

Finally, substituting (5-37) into (5-29) yields:

$$P_{e,bit} \leq \sum_{q=1}^{M^2} \sum_{\hat{q}=1}^{M^2} \frac{N_{st} N(\boldsymbol{x}_q, \boldsymbol{x}_{\hat{q}}) \mu_{\alpha}^{2N_r} \sum_{w=0}^{2N_r-1} \binom{2N_r-1+w}{w} [1-\mu_{\alpha}]^{w}}{M^2} \tag{5-38}$$

5.4 Analytical and Simulated BER Comparison

The aim of this section is to validate the theoretical performance bound derived in (5-38). Monte Carlo simulations are performed over an i.i.d Rayleigh flat fading channel with AWGN, where the average BER is plotted against the average SNR at each receive antenna. The following were assumed during simulation: the channel matrix $\boldsymbol{H}$ and AWGN vector $\boldsymbol{n}$ comprise i.i.d entries distributed according to $\mathcal{CN}(0,1)$; full channel knowledge at receiver; transmit and receive antennas are separated wide enough to avoid correlation; constant fading coefficients over two consecutive time slots and the total transmit power is the same for all transmissions.

The analytical and simulated average BER for 4×4 and 4×2 BPSK ACSM is shown in Figure 5-2. In all results, it is clear that the theoretical upper bounds are increasingly tight at high SNR values, thereby validating analytical frameworks.

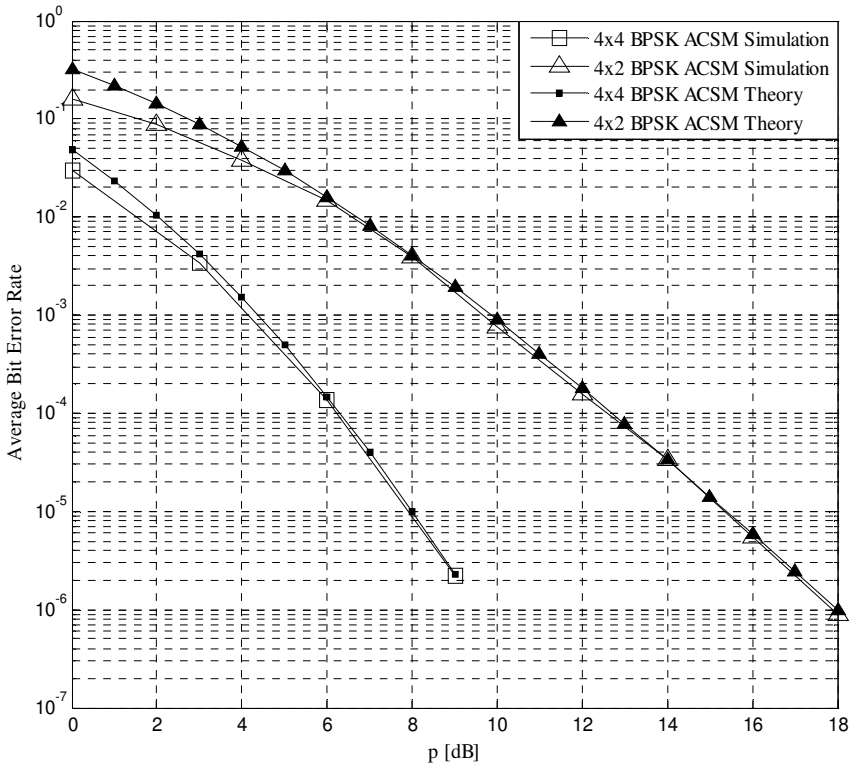

Figure 5-2 Analytical and Simulated BER Comparison

5.5 Performance Comparison: ACSM, Alamouti STBC and SM-OD

The average BER performance of ACSM, Alamouti STBC and SM-OD are compared in this section. The simulation parameters and assumptions are consistent with those defined in Section 5.4. The simulated BER of 4×4 BPSK ACSM, 2×4 4-QAM Alamouti STBC and 2×4 BPSK SM-OD are shown in Figure 5-3. In order to ensure a fair comparison between the various schemes the following transmission setup is used:

- 2 bps data transmission
- 4 receive antennas ($N_r = 4$)
- The total transmit power from two antennas (ACSM and Alamouti STBC) is the same as that transmit power from a single transmit antenna (SM-OD).

It can be seen that ACSM exhibits performance gains of approximately 5.5 dB over SM-OD at a BER of 10^{-5}. The improved performance can be attributed to the fact that ACSM achieves both transmit and receive diversity whereas SM-OD achieves only receive diversity. Also, ACSM outperforms Alamouti STBC by approximately 1.5 dB at a BER of 10^{-5}.The enhanced performance is due to the fact that ACSM uses a lower order digital

modulation scheme (BPSK, M = 2) as compared to Alamouti STBC (4-QAM, M = 4). The ACSM technique utilizes the transmit antenna set index as an additional source of information. As a result, ACSM schemes require lower order constellation size in order to achieve the same transmission rate as an equivalent Alamouti STBC system.

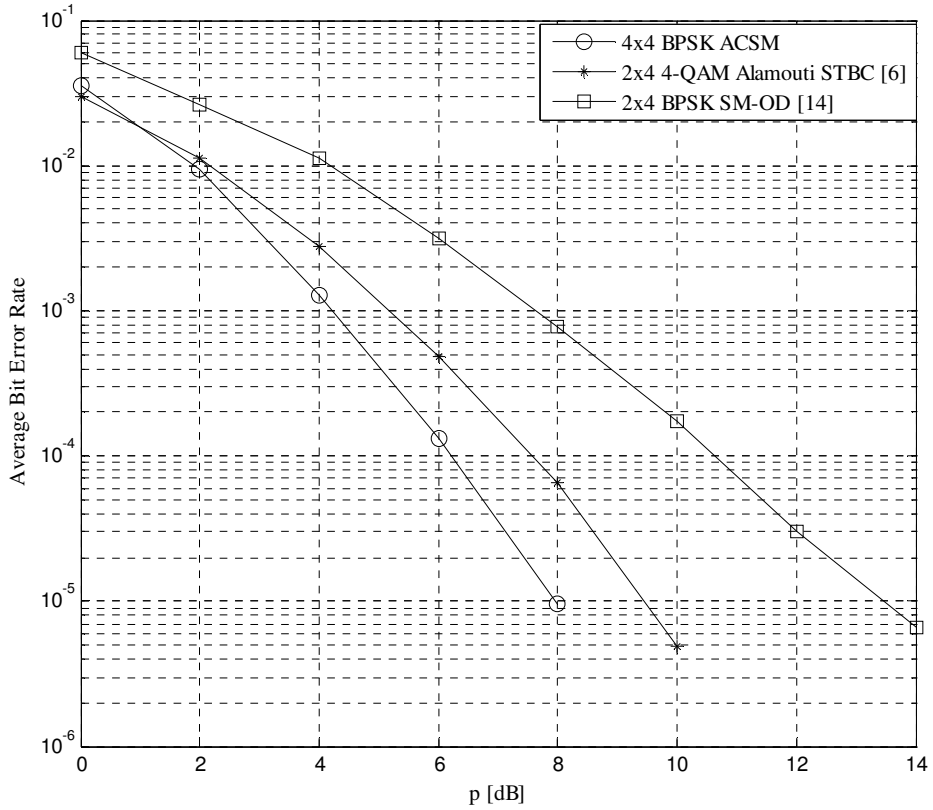

Figure 5-3 ACSM, Alamouti STBC and SM-OD Performance Comparison

5.5 Chapter Summary

In this chapter, a performance enhanced SM technique was proposed and analyzed. The ACSM scheme modifies the conventional SM approach by utilizing Alamouti STBC in conjunction with SM. As a result, ACSM achieves both transmit and receive diversity as compared to conventional SM where only receive diversity is achieved. A closed form analytical performance bound for real constellation ACSM in i.i.d Rayleigh flat fading channels was derived and Monte Carlo simulations were used to demonstrate the accuracy of the theoretical bound. Further simulations show that ACSM performance surpasses that of SM-OD and Alamouti STBC by approximately 5.5 dB and 1.5 dB, respectively. Complexity analyses show that the ACSM scheme requires additional processing at the receiver as compared to SM-OD and Alamouti STBC. However, the increase in computational complexity is traded off by the significant performance gains achievable by ACSM.

It should be noted that STBC-SM, a scheme similar to ACSM has been developed independently in [25]. However, the two schemes differ in terms of mapping table, detection and approach to performance analysis. These differences can be summarized by the following points:

- **Mapping:** The mapping tables are defined differently for each scheme. The ACSM mapping table assigns an r bit binary input to a transmit antenna set index and symbol pair, whereas the STBC-SM mapping table assigns the r bit binary input to a unique transmission matrix [25].
- **Detection:** Both ACSM and STBC-SM schemes utilize ML based detection. However, the ACSM detector performs a joint detection of transmit antenna set index and symbol vector. Alternatively, the STBC-SM detector separates the transmit antenna and symbol detection processes.
- **Performance Analysis:** Both schemes apply the union bound technique [32] in order to obtain an upper bound on the average BER. However, the definition of the bound differs for each system, which is evident from (5-29) and [25, Eq. (20)]. In addition, the ACSM analysis computes the PEP term (5-36) using the probability density function approach [34], whereas the STBC-SM analysis uses the moment generating function approach [34] for computation of the PEP [25, Eq. (22)].

Chapter 6

Conclusion and Future Work

6.1 Conclusion

The main contributions presented in this dissertation can be summarized as follows:

An asymptotic bound for the average BER of M-QAM spatial modulation with optimal based detection in i.i.d Rayleigh flat fading channels was derived in Chapter 3. The analysis assumes independent transmit antenna index and symbol estimation processes, this leads to a lower bound since both processes are practically dependent. The accuracy of the performance bound was substantiated via Monte Carlo simulation results, which show the derived lower bounds to be tight in the high SNR region.

The multiple-stage detection scheme was proposed in Chapter 4. The MS detector aims at reducing the high computational complexity inherent to optimal SM detection for high order M-QAM ($M \geq 16$) configurations. The basic idea behind MS is to divide the SM detection process into two stages. The first stage uses the low complexity sub-optimal (MRRC) SM detector to select the N $(N \leq N_t)$ most probable estimates of transmit antenna index, thereby reducing the number of possible inputs pairs from $N_t M$ to NM. In the second stage, the reduced input set is sent to the optimal (ML) SM detector, which computes a final estimate of transmit antenna index ($\hat{j}_{MS}$) and transmitted symbol ($x_{\hat{q}_{MS}}$). Since the NM input pairs to the second stage are the most probable estimates of transmit antenna index and modulated symbol, the high performance inherent to SM-OD is still maintained. Monte Carlo simulations and complexity analyses have shown that MS detection provides an efficient method for attaining near optimal performance with significantly reduced receiver complexity (up to 35% reduction) as compared to the SM-OD scheme.

A performance enhanced SM technique was presented in Chapter 5. The ACSM technique modifies the conventional SM approach by utilizing Alamouti STBC in conjunction with SM. As a result, ACSM obtains a higher diversity gain as compared to conventional SM. The advantages and disadvantages of ACSM can be summarized as follows:

Advantages:

- **Transmit Diversity**: The ACSM scheme utilizes Alamouti STBC and therefore obtains transmit diversity.
- **Receive Diversity**: Multiple antenna reception provides receive diversity.
- **ICI Avoidance**: ACSM data transmission is based on Alamouti's scheme, which is orthogonal by design. Hence, ACSM is not prone to the detrimental effects of ICI.
- **Enhanced Spectral Efficiency**: ACSM encodes data in the transmit antenna set index, thereby increasing spectral efficiency by the base two logarithm of the total number of transmit antenna sets.
- **Performance**: The ACSM scheme offers performance gains of approximately 1.5 dB and 5.5 dB over Alamouti STBC and SM-OD schemes, respectively.

Disdavantages:

- **IAS**: The ACSM scheme requires IAS to ensure the simultaneous transmission of data from both antennas.
- **Complexity**: The ML based ACSM detector has a high computational complexity as compared to SM-OD and Alamouti STBC.
- **Restricted Antenna Set**: The ACSM scheme works only for a number of transmit antenna sets which are a power of two.

A theoretical performance bound to quantify the average BER of real constellation ACSM over i.i.d Rayleigh flat fading channels was also derived in Chapter 5. It was demonstrated that the theoretical performance bound is increasingly tight in the high SNR region, thereby validating analytical frameworks.

6.2 Future Work

Future work aims at providing research advances in the following directions:

- The analysis performed in Chapter 5 is specific to real constellation ACSM configurations. Therefore, a possible extension of this analysis to cater for M-QAM ACSM schemes is to be explored.

- The idealized assumption of Rayleigh flat fading channels is not suitable in real world scenarios. Therefore, it is desirable to investigate the performance of ACSM under non-ideal channel conditions such as correlated fading.

- The ACSM detector is impractical due to its high computational complexity. Hence, the research into an alternate low complexity ACSM detection scheme is necessary. One idea is to apply the sub-optimal sphere decoding technique. However, the ACSM scheme randomly selects the transmit antenna set index, which makes direct application of the sphere decoding algorithm difficult.

Appendix A

The received signal vector is given by:

$$\boldsymbol{y} = \sqrt{p}\boldsymbol{h}_j x_q + \boldsymbol{n} \tag{A-1}$$

where $\boldsymbol{y} = [\, y_1\ y_2 \ldots y_{N_r}]^T$ is the received signal vector, p is the average SNR at each receive antenna, $\boldsymbol{h}_j$ denotes the j^{th} column of $\boldsymbol{H}$, x_q corresponds to the q^{th} symbol from an M-ary constellation and $\boldsymbol{n} = [n_1\ n_2 \ldots\ n_{N_r}]^T$ is the N_r dimensional AWGN vector.

The derivation of (3-6) is as follows:

$$P(\boldsymbol{x}_{jq} \to \boldsymbol{x}_{\hat{j}q} | \boldsymbol{H}) = P\left(\left\| \boldsymbol{y} - \sqrt{p}\boldsymbol{h}_{\hat{j}} x_q \right\|_F < \left\| \boldsymbol{y} - \sqrt{p}\boldsymbol{h}_j x_q \right\|_F \right) \tag{A-2}$$

Substituting (A-1) in (A-2) yields:

$$\begin{aligned} P(\boldsymbol{x}_{jq} \to \boldsymbol{x}_{\hat{j}q} | \boldsymbol{H}) &= P\left(\left\| \sqrt{p}\boldsymbol{h}_j x_q + \boldsymbol{n} - \sqrt{p}\boldsymbol{h}_{\hat{j}} x_q \right\|_F < \left\| \sqrt{p}\boldsymbol{h}_j x_q + \boldsymbol{n} - \sqrt{p}\boldsymbol{h}_j x_q \right\|_F \right) \\ &= P\left(\left\| \left(\sqrt{p}\boldsymbol{h}_j x_q - \sqrt{p}\boldsymbol{h}_{\hat{j}} x_q \right) + \boldsymbol{n} \right\|_F < \|\boldsymbol{n}\|_F \right) \end{aligned} \tag{A-3}$$

The triangle inequality states that [35]:

$$\left\| \sqrt{p}\boldsymbol{h}_j x_q - \sqrt{p}\boldsymbol{h}_{\hat{j}} x_q \right\|_F - \|\boldsymbol{n}\|_F \le \left\| \left(\sqrt{p}\boldsymbol{h}_j x_q - \sqrt{p}\boldsymbol{h}_{\hat{j}} x_q \right) + \boldsymbol{n} \right\|_F \le \left\| \sqrt{p}\boldsymbol{h}_j x_q - \sqrt{p}\boldsymbol{h}_{\hat{j}} x_q \right\|_F + \|\boldsymbol{n}\|_F$$

Hence,

$$P(\boldsymbol{x}_{jq} \to \boldsymbol{x}_{\hat{j}q} | \boldsymbol{H}) = P\left(\left\| \sqrt{p}\boldsymbol{h}_j x_q - \sqrt{p}\boldsymbol{h}_{\hat{j}} x_q \right\|_F - \|\boldsymbol{n}\|_F < \|\boldsymbol{n}\|_F \right) \tag{A-4}$$

$$= P\left(\|\boldsymbol{n}\|_F > \frac{\left\| \left(\sqrt{p}\boldsymbol{h}_j x_q - \sqrt{p}\boldsymbol{h}_{\hat{j}} x_q \right) \right\|_F}{2} \right)$$

Therefore, the conditional pairwise error probability (A-4) is equivalent to the probability that noise vector $\boldsymbol{n}$ lies closer to the vector $\left(\sqrt{p}\boldsymbol{h}_j x_q - \sqrt{p}\boldsymbol{h}_{\hat{j}} x_q \right)$ than to the origin. This

probability is dependent solely on the projection of $\boldsymbol{n}$ onto the line joining the origin and the point $\sqrt{p}\boldsymbol{h}_j x_q - \sqrt{p}\boldsymbol{h}_{\hat{j}} x_q$ [27, pp. 138-139], as shown in Figure A-1 [redrawn from 20].

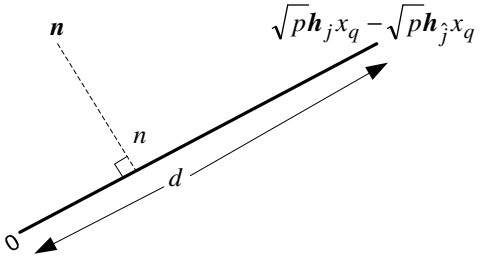

Figure A-1. Noise projection

The projection of $\boldsymbol{n}$ onto this one dimensional line is a one dimensional Gaussian random variable n distributed according to $\mathcal{N}(0, 1/2)$.

Thus,

$$P(\boldsymbol{x}_{jq} \to \boldsymbol{x}_{\hat{j}q} | \boldsymbol{H}) = P\left(n > \frac{d}{2}\right) = \frac{1}{\sqrt{2\pi\sigma^2}} \int_{d/2}^{\infty} exp\left(-\frac{v^2}{2\sigma^2}\right) dv = Q\left(\frac{d}{2\sigma}\right) \tag{A-5}$$

where $d = \left\|\left(\sqrt{p}\boldsymbol{h}_j x_q - \sqrt{p}\boldsymbol{h}_{\hat{j}} x_q\right)\right\|_F$

Substituting $\sigma = \frac{1}{\sqrt{2}}$ in (A-5) yields:

$$P(\boldsymbol{x}_{jq} \to \boldsymbol{x}_{\hat{j}q} | \boldsymbol{H}) = Q\left(\frac{d}{\sqrt{2}}\right) = Q\left(\sqrt{\frac{p}{2}} \left\|\left(\boldsymbol{h}_j x_q - \boldsymbol{h}_{\hat{j}} x_q\right)\right\|_F\right) \tag{A-6}$$

Let $k = \frac{p}{2} \left\|\left(\boldsymbol{h}_j x_q - \boldsymbol{h}_{\hat{j}} x_q\right)\right\|_F^2$

Then,

$$P(\boldsymbol{x}_{jq} \to \boldsymbol{x}_{\hat{j}q} | \boldsymbol{H}) = Q(\sqrt{k}) \tag{A-7}$$

References

[1] C. E. Palazzi, M. Roccetti and S. Ferretti, “An intervehicular communication architecture for safety and entertainment,” *IEEE Trans. Intell. Transp. Syst.*, vol. 11, no. 1, pp 90-99, Mar. 2010.

[2] E. Telatar, “Capacity of multi-antenna Gaussian channels,” *Eur. Trans. Telecommun.*, vol. 10, no. 6, pp. 558–595, Nov. 1999.

[3] G. J. Foschini and M. J. Gans, “On limits of wireless communications in a fading environment when using multiple antennas,” *Wireless Personal Commun*., vol. 1, no. 6, pp. 311–335, Mar. 1998.

[4] R. Ran, J. Yang and D. Kim, “Multimode precoder design for STBC with limited feedback in MIMO based wireless communication system,” *IEICE Electron. Express*, vol. 1, no. 2, pp. 222-229, Jun. 2005.

[5] V. Tarokh, N. Seshadri and A. Calderbank, “Space-time codes for high data rate wireless communication: Performance criterion and code construction,” *IEEE Trans. Inform. Theory*, vol. 44, no. 2, pp. 744–765, Mar. 1998.

[6] S. Alamouti, “A simple transmit diversity technique for wireless communications,” *IEEE J. Select. Areas Commun.*, vol. 16, no. 8, pp. 1451–1458, Oct. 1998.

[7] J. Jeganathan, “Space shift keying modulation for MIMO channels,” M.S thesis, Concordia University, Montreal, Quebec, Canada, Aug 2008.

[8] P. Wolniansky, G. Foschini, G. Golden and R. Valenzuela, “V-BLAST: An architecture for realizing very high data rates over the rich- scattering wireless channel,” in *Proc. URSI Int. Symp. on Signals, Systems and Electronics*, Pisa, Italy, pp. 295–300, Sept. 1998.

[9] S. Haykin and M. Moher, *Modern Wireless Communications*, 5th ed. New Jersey: Prentice-Hall, 2003.

[10] A. Goldsmith, S. Jafar, N. Jindal and S. Vishwanath, “Capacity limits of MIMO channels,” *IEEE J. Sel. Areas Commun.*, vol. 21, no. 5, pp. 684–702, Jun. 2003.

[11] M. Damen, A. Abdi and M. Kaveh, “On the effect of correlated fading on several space-time coding and detection schemes,” in *Proc. IEEE Veh. Technol. Conf.*, Atlantic City, pp. 13-16, Oct. 2001.

[12] R. Mesleh, H. Haas, C. W. Ahn and S. Yun, "Spatial Modulation - A new low complexity spectral efficiency enhancing technique," in *Proc. ChinaCOM*, Beijing, China, pp. 1-5, Oct. 2006.

[13] R. Mesleh, H. Haas, S. Sinanovic, C. W. Ahn and S. Yun, “Spatial modulation,” *IEEE Trans. Veh. Technol.*, vol. 57, no.4, pp. 2228-2241, Jul. 2008.

[14] J. Jeganathan, A. Ghrayeb and L. Szczecinski, “Spatial modulation: optimal detection and performance analysis,” *IEEE Commun. Lett.,* vol. 12, no. 8, pp. 545-547, Aug. 2008.

[15] J. Jeganathan, A. Ghrayeb, L. Szczecinski and A. Ceron, “Space shift keying modulation for MIMO channels,” *IEEE Trans. Wireless Commun.*, vol. 8, no. 7, pp. 3692-3703, Jul. 2009.

[16] J. Jeganathan, A. Ghrayeb, and L. Szczecinski, “Generalized space shift keying modulation for MIMO channels,” in *Proc IEEE Int. Symp. Personal, Indoor, Mobile Radio Commun.*, Cannes, France, pp. 1–5, Sept. 2008.

[17] N. Serafimovski, M. Di Renzo, S. Sinanovic, R. Mesleh and H. Haas, “Fractional bit encoded spatial modulation,” *IEEE Commun. Lett.,* vol. 14, no. 5, pp. 429-431, May 2008.

[18] R. Mesleh, I. Stefan, H. Haas and P. M. Grant, “On the performance of trellis coded spatial modulation,” in *Proc. Int. ITG Workshop on Smart Antennas*, Berlin, Germany, pp. 235–241, Feb. 2009.

[19] M. Di Renzo, R. Mesleh, H. Haas and P. M. Grant, “Upper bounds for the analysis of trellis coded spatial modulation over correlated fading channels,” in *Proc. IEEE Veh. Technol. Conf.*, Taipei, Taiwan, pp. 1-5, May 2010.

[20] S. Hwang, S. Jeon, S. Lee and J. Seo, “Soft-output ML detector for OFDM spatial modulation systems,” *IEICE Electronics Express*, vol. 6, no.19, pp. 1426-1431, Sept. 2009.

[21] M. Di Renzo and H. Haas, "Spatial modulation with partial-CSI at the receiver: optimal detector and performance evaluation," in *Proc IEEE 33rd Conf. Sarnoff.*, New Jersey, pp. 1-6, Apr. 2010.

[22] R. Mesleh, R. Mehmood, R. Elgala and H. Haas, "Indoor MIMO optical wireless communication using spatial modulation," in *Proc. IEEE ICC. Conf.*, Cape Town, South Africa, pp. 1-5, May 2010.

[23] R. Mesleh, H. Elgala and H. Haas, "On the performance of coded optical spatial modulation," in *Proc. IEEE 21st Int. Symp. Personal Indoor and Mobile Radio,* Instanbul, Turkey, pp. 820-824, Sept. 2010.

[24] G. Mingxi, J. Chong and S. Yuehong, "Detection algorithm for spatial modulation system under unconstrained channel," in *Proc IEEE 12th Int. Conf. Commun. and Technol.*, Nanjing, China, pp. 458-461, Nov. 2010.

[25] E. Basar, U. Aygolu, E. Panayirci, H. Poor, "Space-time block coded spatial modulation," *IEEE Trans. Commun.*, vol. 59, no. 3, pp. 823-832, Mar. 2011.

[26] H. Suzuki, "A statistical model for urban radio propagation," *IEEE Trans. Commun.*, vol. COM-25, no. 7, pp. 673-680, Jul. 1977.

[27] A. J. Goldsmith, *Wireless Communications*, 1st ed. New York: Cambridge University Press, 2005.

[28] R. Mesleh, "Spatial Modulation: A spatial multiplexing technique for efficient wireless data transmission," Ph.D dissertation, Jacobs University, Bremen, Germany, Jun. 2007.

[29] R. Mesleh, S. Engelken, S. Sinanovic and H. Haas, "Analytical SER calculation of spatial modulation," in *Proc. of the IEEE 10th Int. Symp. on Spread Spectrum Technologies and Applications*, Bologna, Italy, pp. 272-276, Aug. 2008.

[30] H. Xu, "Symbol Error Probability for generalized selection combining reception of *M*-QAM," *SAIEE Africa Research Journal*, vol. 100, no.3, pp. 68-71, Sept. 2009.

[31] I. Al-Shahrani, "Performance of *M*-QAM over generalized mobile fading channels using MRC diversity," M.S thesis, King Saud University, Riya, Saudi Arabia, Feb. 2007.

[32] J. G. Proakis, *Digital Communications*, 4th ed. New York: McGraw-Hill, 2001.

[33] M. S. Alouini and A. J. Goldsmith, “A unified approach for calculating error rates of linearly modulated signals over generalized fading channels,” *IEEE Trans. Commun.*, vol. 47, no. 9, pp. 1324–1334, Sept. 1999.

[34] M. S. Alouini and M. K. Simon, *Digital Communications over Fading Channels*, 2nd ed. New York: John & Wiley, 2005.

[35] F. Beauregard, *Linear Algebra*, 3rd ed. New York: Prentice-Hall, 1995.